Constraining CO_2 emissions from open biomass burning by satellite observations of co-emitted species: a method and its application to wildfires in Siberia

I. B. Konovalov[1,2], E. V. Berezin[1,2], P. Ciais[3], G. Broquet[3], M. Beekmann[4], J. Hadji-Lazaro[5], C. Clerbaux[5], M. O. Andreae[6], J. W. Kaiser[6,7,8], and E.-D. Schulze[9]

[1]Institute of Applied Physics, Russian Academy of Sciences, Nizhniy Novgorod, Russia

[2]Lobachevsky State University of Nizhny Novgorod, Nizhny Novgorod, Russia

[3]Laboratoire des Sciences du Climat et l'Environnement (LSCE/IPSL), CNRS-CEA-UVSQ, Centre d'Etudes Orme des Merisiers, Gif sur Yvette, France

[4]Laboratoire Inter-Universitaire de Systèmes Atmosphériques (LISA/CNRS), CNRS, UMR7583, Université Paris-Est and Université Paris 7, Créteil, France

[5]UPMC Univ. Paris 06; Université Versailles St-Quentin; CNRS/INSU, LATMOS-IPSL, Paris, France

[6]Biogeochemistry Department, Max Planck Institute for Chemistry, Mainz, Germany

[7]King's College London (KCL), London, UK

[8]European Centre for Medium-range Weather Forecasts (ECMWF), Reading, UK

[9]Max Planck Institute for Biogeochemistry, Jena, Germany

Correspondence to: I. B. Konovalov (konov@appl.sci-nnov.ru)

Abstract. A method to constrain carbon dioxide (CO_2) emissions from open biomass burning by using satellite observations of co-emitted species and a chemistry-transport model (CTM) is proposed and applied to the case of wildfires in Siberia. CO_2 emissions are assessed by means of an emission model assuming a direct relationship between the biomass burning rate (BBR) and the Fire Radiative Power (FRP) derived from MODIS measurements. The key features of the method are (1) estimating the FRP-to-BBR conversion factors (α) for different vegetative land cover types by assimilating the satellite observations of co-emitted species into the CTM, (2) optimal combination of the estimates of α derived independently from satellite observations of different species (CO and aerosol in this study), and (3) estimation of the diurnal cycle of the fire emissions directly from the FRP measurements. Values of α for forest and grassland fires in Siberia and their uncertainties are estimated using IASI carbon monoxide (CO) retrievals and MODIS aerosol optical depth (AOD) measurements combined with outputs from the CHIMERE mesoscale chemistry-transport model. The constrained CO emissions are validated through comparison of the respective simulations with independent data of ground based CO measurements at the ZOTTO site. Using our optimal regional-scale estimates of the conversion factors (which are found to be in agreement with earlier published estimates obtained from local measurements of experimental fires), the total CO_2 emissions from wildfires in Siberia in 2012 are estimated to be in the range from 280 to 550 Tg C, with the optimal (maximum likelihood) value of 392 Tg C. Sensitivity test cases featuring different assumptions regarding the injection height and diurnal variations of emissions indicate that the derived estimates of the total CO_2 emissions in Siberia are robust with respect to the modelling options (the different estimates vary within less than 15 % of their magnitude). The CO_2 emission estimates obtained for several years are compared with independent estimates provided by the GFED3.1 and GFASv1.0 global emission inventories. It is found that our "top-down" estimates for the total annual biomass burning CO_2 emissions in the period from 2007 to 2011 in Siberia are by factors of 2.5 and 1.8 larger than the respective bottom-up estimates; these discrepancies cannot be fully explained by uncertainties in our estimates. There are also considerable differences in the spatial distribution of the different emission estimates; some of those differences have a systematic character and require further analysis.

1 Introduction

Wildfires occurring either naturally or ignited by humans strongly affect the atmospheric composition and thermal balance on both the global and regional scales by providing major sources of greenhouse and reactive gases and aerosols (e.g., Andreae and Merlet, 2001; IPCC, 2007, Langmann et al., 2009; Jaffe et al., 2012; Bond et al., 2013). Wildfires are a key component of the global carbon cycle: they are not only causing the immediate release of carbon stored in vegetation into the atmosphere, but they also induce a long-term shift in the balance between the carbon sequestration by plants and carbon liberation through decomposition of dead biomass (Lorenz and Lal, 2010). The impact of fires on the carbon cycle can become especially important in the situation of continuing climate change, as global warming is expected to change fire regimes and may accelerate the accumulation of carbon dioxide (CO_2), methane, and ozone precursors in the atmosphere, thus leading to further warming (Bond-Lamberty et al., 2007). Accurate estimation of such climatic feedbacks through fires can hardly be possible without adequate quantitative knowledge of the CO_2 emissions from wildfires.

Presently, estimates of emissions of CO_2 and other species from wildfires and other types of open biomass burning are available on the global scale from several "bottom-up" emission inventories, such as, e.g., the Global Fire Emission Database (GFED) (van der Werf et al., 2010; Giglio et al., 2013), the Wildland Fire Emission Inventory (WFEI) (Urbanski et al., 2011), the Emissions for Atmospheric Chemistry and Climate Model Intercomparison Project (ACCMIP) inventory (Lamarque et al., 2010), the Fire INventory from NCAR (FINN) (Wiedinmyer et al., 2011) and the Global Fire Assimilation System (GFAS) emission data set (Kaiser et al., 2012). Such inventories are based on different kinds of available satellite data (e.g., burnt area, hot spots, or fire radiative power) which are used to characterize time, location, and the size or intensity of fires. The emission estimates provided by the bottom-up inventories may involve considerable uncertainties caused by uncertainty in the satellite measurement data, as well as by uncertainties in additional data (such as available "fuel" amounts and combustion efficiencies) and parameters establishing a relationship between the satellite data and the emissions of a given species (e.g., Wiedinmyer et al., 2006; van der Werf et al., 2010). Although not all of the inventories may be considered as being fully independent of each other, a part of these uncertainties are evidenced by discrepancies between the data of different inventories (Kaiser et al., 2012; Petrenko et al., 2012).

A common way to validate emission inventories involves using the inventory data in atmospheric chemistry and transport models and comparing the model outputs with atmospheric measurements of some emitted species. Studies using this approach in the case of biomass burning emissions are numerous (e.g., Park et al., 2003; Turquety et al., 2007; Hodzic et al., 2007; Jeong et al., 2008; Pfister et al., 2008; Sofiev et al., 2009; Larkin et al., 2009; Ito, 2011; Huijnen et al., 2012; Kaiser et al., 2012). Some of the modelling studies revealed systematic discrepancies between the measured and simulated data and attributed a part of them to uncertainties in biomass burning emission data (Wang et al., 2006; Singh et al., 2012; Hodnebrog et al., 2012; Petrenko et al., 2012). Several studies employed more sophisticated inverse modelling methods to constrain uncertainties of the bottom-up biomass burning emission data and to provide top-down emission estimates derived from observations of atmospheric composition. Most studies have mainly been focused on constraining carbon monoxide (CO) (Pfister et al., 2005; Arellano et al., 2006; Hooghiemstra et al., 2012; Krol et al., 2013) or aerosol emissions (Zhang et al., 2005; Dubovic et al., 2008; Huneeus et al., 2012; Schutgens et al., 2012; Xu et al., 2013), whereas there is less work focusing on constraining CO_2 emissions.

While inverse modelling methods have also been widely used for estimation of CO_2 fluxes in different regions by using both ground based (see, e.g., Enting, 2002 and references therein; Gurney et al., 2002; Rayner et al., 2008; Ciais et al., 2010) and, more recently, satellite measurements of CO_2 mixing ratios (e.g., Chevallier et al., 2009; Nassar et al., 2011; Saeki et al., 2013), they usually do not allow identifying CO_2 sources associated with biomass burning separately due to, in particular, strong interference by other major natural sources and sinks of carbon dioxide such as soil and plant respiration and photosynthesis (IPCC, 2007) and the lack of explicit inclusion of fire CO_2 emissions in inversion prior fluxes. Solution of the typically ill-conditioned inverse problems (Enting et al., 2002) with respect of CO_2 fluxes is further hindered by the long life time of CO_2 and its the relatively small variability in the atmosphere, leading to a rather strong sensitivity of emission estimates to model and measurement errors (e.g. Houweling et al., 2010).

A promising approach to constrain CO_2 emissions from specific sources involves using measurements of other co-emitted species (tracers) in situations where the main sources of the tracers and CO_2 are essentially the same (Suntharalingam et al., 2004; Rivier et al., 2006). The methods developed within this approach range from analysis of the relationships between observed concentrations of CO_2 and co-emitted species (Suntharalingam et al., 2004; Rivier et al., 2006; Palmer et al., 2006; Brioude et al., 2012) to a combination of top-down estimates of tracer emissions with information provided by bottom-up emission inventories (Berezin et al., 2013). So far, such methods have only been applied to estimation of CO_2 emissions from fossil fuel burning.

The method presented in this paper follows the above-mentioned approach and aims at inferring pyrogenic CO_2 emission estimates from satellite measurements of CO and aerosol optical depth (AOD). Although the concepts underlying the method described in this paper and of the method applied earlier by Berezin et al. (2013) to study multi-annual

relative changes of anthropogenic CO$_2$ emissions in China are similar, the methods themselves are different due to fundamental differences in the problems addressed. The core of the method employed in this study is the use of the fire radiative power (FRP) (Ichoku and Kaufman, 2005) to derive the spatial and temporal structure of the biomass burning rate (here, this is the amount of dry biomass (g) burned per second; for brevity, this characteristic, which essentially represents the total carbon emission rate, is referred to as BBR below). Similar to several other modelling studies (Pereira et al., 2009; Sofiev et al., 2009; Konovalov et al., 2011; 2012; Kaiser et al., 2012; Huijnen et al., 2012) employing FRP measurements, the emissions of a given species are obtained as the product of BBR and a corresponding emission factor.

A serious problem associated with the application of FRP measurements for the estimation of emissions from biomass burning concerns the evaluation of the empirical coefficients providing conversion of FRP to BBR (these coefficients are referred below for brevity to as the FRP-to-BBR conversion factors). Although such conversion factors can, in principle, be evaluated directly in local experiments (Wooster et al., 2005), it is not obvious that the local relationship between the BBR in real wildfires and FRP measured from space during a period of months to years and over a large region with diverse ecosystems should be the same as that measured during fire experiments. On the one hand, some biases in FRP measured from space may be associated, in particular, with the effects of clouds and heavy smog; on the other hand, surface fires in forests can be obscured by tree crowns, and will not or only partially be seen in FRP measurements from space. One of the main features of our method is the use of satellite CO and AOD observations to estimate the FRP-to-BBR conversion factors for different vegetative land cover types by optimizing the agreement between the CO and AOD observations and corresponding simulations. In this way, we can also verify that the optimized emissions of CO and aerosols are consistent (within the range of indicated uncertainties) with the corresponding observations. Another important element of our method is the optimal (probabilistic) combination of the FRP-to-BBR conversion factors estimated independently from the satellite observations of each different species. The estimates of the FRP-to-BBR conversion factors derived separately from CO and AOD measurements can be used for their mutual cross validation, while the probabilistic combination of the estimates using both CO and AOD yields the dual-constrained optimal estimates featuring the reduced uncertainty brought by combining CO and AOD constraints. Indirect top-down CO$_2$ emission estimates are then obtained after applying CO$_2$ emission factors to the optimized spatial-temporal fields of the biomass burning rate.

It may be useful to mention some ways to infer emissions of a given species from FRP measurements, which have been used in other studies. In particular, Ichoku and Kaufman (2005), and Pereira et al. (2009) approximated a statistical relationship between FRP and aerosol emission rates derived from simultaneous AOD measurements under some simplified assumptions. A similar, but more sophisticated method involving aerosol sources distributed in space and time by inverse modelling was used by Vermote et al. (2009). Kaiser et al. (2012) calibrated their FRP-based emission estimates in the framework of the GFASv1.0 emission inventory with the data of another global bottom-up emission inventory (GFED3.1) based on burned area data and other parameters from a diagnostic biosphere model. Finally, similar to the approach used in this study, Sofiev et al. (2009) and Konovalov et al. (2011) calibrated empirical relationships between FRP and emissions of a given species by optimizing the agreement between its atmospheric observations and corresponding simulations; however, unlike in the present study, only near-surface concentration data were used in those studies for the calibration.

We apply our novel method to estimate CO$_2$ emissions from wildfires in Siberia. The processes (such as wildfires) affecting the carbon balance in the Siberian region are important components of the regional and global carbon cycle, as the Siberian boreal forest contains around 25 % of global terrestrial biomass (Conard et al., 2002). Accurate estimates of pyrogenic CO$_2$ fluxes (directly related to the amounts of biomass burned) are requisite for reliable examination of both direct and indirect effects of Siberian fires on atmospheric composition and climate change. Meanwhile, significant discrepancies between published estimates of pyrogenic emissions in Russia indicate that the knowledge of CO$_2$ emissions from Siberian wildfires is currently rather deficient. In particular, the annual estimates (based on burnt area data) provided for the total carbon emissions from Russian wildfires (occurring mainly in Siberia) by Shvidenko et al. (2011) and Dolman et al. (2012) differ in some years by more than a factor of two from the corresponding estimates provided by the global GFED3 inventory (van der Werf et al., 2010). Large potential uncertainties in pyrogenic emission inventory data for Siberia were also indicated by Soja et al. (2004) and Kukavskaya et al. (2013). As discussed in Shvidenko et al. (2011), the discrepancies between the results of the different inventories are not only due to differences in the assessment methods but, most importantly, due to the varying degree of the completeness and reliability of the initial data (concerning, in particular, the burnt area and the basic biophysical characteristics of the vegetation).

Accordingly, one of the main goals of this study is to obtain top-down estimates for the total CO$_2$ emissions from wildfires in Siberia. Our estimates are to a significant extent independent of estimates provided by bottom-up inventories, since the only "a priori" information (apart from the data provided by satellite measurements and a chemistry-transport model) used in our estimation method are the ratios of the emission factors for the tracers considered to those for CO$_2$. The estimates obtained for several years (2007–2012) are compared to the data from two widely used global emission inventories, namely GFED3.1 (van der Werf et al., 2010)

and GFASv1.0 (Kaiser et al., 2012); these inventories are not completely independent of one another, as the latter involves linear regressions to GFED3.1 as a part of the estimation procedure.

The paper is organized as follows. Our method is explained in detail in Sect. 2. Measured and simulated data employed in our analysis are described in Sect. 3. The results, including inferred optimal estimates of the FRP-to-BBR conversion factors, total CO_2 emissions from wildfires in Siberia, and their comparison with the corresponding data from the GFED3.1 and GFASv1.0 inventories are presented in Sect. 4. Finally, the main findings of our study are summarized in Sect. 5.

2 Optimization of fire emission estimates: method description

2.1 FRP data and basic formulations

To characterize fire intensity, we use the Fire Radiative Power (FRP) data retrieved from the MODIS infrared measurements on-board the Aqua and Terra satellites. The FRP data were available from the standard MODIS L2 "Thermal anomalies & Fire" data product (MOD14 and MYD14) provided by the NASA Land Processes Distributed Active Archive Center (LP DAAC) through the Earth Observing System (EOS) Clearinghouse (ECHO) (http://reverb.echo.nasa.gov). The swath data were provided for each satellite overpass at the nominal 1 km resolution. The data were acquired twice a day by both the Aqua (at 1.30p.m. and a.m.) and Terra (10.30a.m. and p.m.) satellites. The details on the retrieval algorithm can be found elsewhere (Kaufman et al., 1998; Justice et al., 2002). The uncertainties in the FRP data are difficult to quantify in a general way because they are strongly dependent on meteorological conditions (since satellites cannot detect fires obscured by clouds) and the temporal evolution of the fires (since a satellite normally overpasses the same territory only twice a day).

Similar to Kaiser et al. (2009a, b, 2012) and Konovalov et al. (2011) we assume the following relationship between the FRP and emissions of a given species in a given cell of a chemistry-transport model grid:

$$E^s(t) = \Phi_d \sum_l \alpha_l \beta_l^s \rho_l h_l(t) \tag{1}$$

where $E^s(t)$ ($\mathrm{g\,s^{-1}\,m^{-2}}$) is the emission rate of a model species s at time t, Φ_d ($\mathrm{W\,m^{-2}}$) is the daily mean FRP density derived from satellite measurements (see Eqs. 2 and 3 below), α_l ($\mathrm{g[dry\,biomass]\,s^{-1}\,W^{-1}}$) are the FRP-to-BBR conversion factors, β_l^s ($\mathrm{g[model\,species]\,g^{-1}[dry\,biomass]}$) are the emission factors, ρ_l is the fraction of the land cover type l, and h_l is the diurnal variation of FRP density. This theoretical relationship defined for a given grid cell is extended to the whole model grid by using the data and assumptions discussed below. In this study, the FRP densities were first calculated on a $0.2° \times 0.1°$ rectangular grid; the daily mean FRP densities estimated with Eq. (2) were then projected onto the $1° \times 1°$ grid of our model (see Sect. 3.2).

Note that, unlike Konovalov et al. (2011), we do not consider peat fires explicitly. However, the emissions from peat fires (at least, from those coinciding on a model grid with fires visible from space) are taken into account in our study implicitly through optimisation of the FRP-to-BBR conversion factors (see Sect. 2.3). Similarly, we take implicitly into account emissions from ground fires occurring underneath a forest canopy and from smouldering fires accompanying visible fires. In this study, we also omitted a correction factor which was introduced in Konovalov et al. (2011) in an ad hoc way to account for possible attenuation of FRP by smoke aerosol during the episode of the extreme air pollution caused by the 2010 Russian fires. We believe that this effect plays a much less important role in the case addressed in this study, and the omission of the correction factor greatly simplifies the analysis. We expect that any variable (in space and time) uncertainties in the FRP data are manifested in our study in the disagreement between the simulated and measured data of atmospheric composition and, eventually, in the reported uncertainties of our emission estimates, while possible systematic uncertainties are compensated as a result of the optimization of the FRP-to-BBR conversion factors.

Similar to Konovalov et al. (2011), we evaluate the daily mean FRP density (Φ_d) by selecting daily maxima of the FRP density in each model grid cell and by scaling them with the assumed diurnal cycle of FRP:

$$\Phi_d = \frac{\max\{\Phi_k, k = 1, \dots K\}}{\sum_l \rho_l h_l(t_{\max})}. \tag{2}$$

Here, $t_{\max}$ is the moment when the maximum FRP density was measured and Φ_k is the FRP density evaluated for each overpass k of any of the considered satellites during a given day:

$$\Phi_k = \frac{\sum_j \mathrm{FRP}_{jk}}{\sum_j S_{jk}^f + S_k^c}, \tag{3}$$

where j is the index of a fire pixel, S_{jk}^f and S_k^c are the area (km^2) of the fire pixels and the remaining observed area (except water) in a given grid cell, respectively. Note that by selecting the daily maxima of FRP we attempt to select the FRP measurements which are least affected (during a given day) by clouds and heavy smoke.

Taking into account the large uncertainties in the available estimates of emission factors (see Sect. 2.5), we considered only three aggregated vegetative land cover categories, i.e., forest (including both coniferous and broadleaf forests), grass (including shrubs), and agricultural land. The fraction of each category per grid cell was calculated by using the Global Land Cover Facility (GLCF) database (Hansen and Reed, 2000), which originally distinguishes 14 land

cover classes. Furthermore, the FRP-to-BBR conversion factors as well as the diurnal variations of FRP and emissions for fires in agricultural land and grass fires were assumed to be the same. This assumption seems to be reasonable in view of the large uncertainties in the obtained estimates of the conversion factor for the "grass" category (see Sect. 4.1), indicating that the available observational information is insufficient for inferring more detailed estimates of the FRP-to-BBR conversion factors. Thus, here we estimate the FRP-to-BBR conversion factors for the two broad categories of vegetative land cover, which for brevity are referred to below as "forest" and "grassland". The spatial distribution of these two categories of vegetative land cover is shown in Fig. 1, which also shows our model domain (see Sect. 3.2).

The optimization of the FRP-to-BBR conversion factors is performed over the period from 1 May to 30 September 2012. This period includes episodes of the unusually intensive Siberian wildfires that, as shown below, led to strong (and clearly detectable from space) perturbations of atmospheric composition over Siberia in July, and also to haze at the North American west coast after transport of smoke across the Northern Pacific (Flemming et al., 2013). The average FPR densities (over the defined period) are shown in Fig. 2a, and the daily variability of the spatially-averaged FRP is demonstrated in Fig. 2b. Evidently, the most intense fires occurred in the central and south-western parts of Siberia, as well as in the Russian far east. The strongest grass and forest fires took place in May, July and August; the contribution to the measured FRP from forest fires was commonly predominating.

Geographically, we limit our analysis (that is, assimilation of atmospheric composition measurements and estimation of total CO$_2$ emissions from fires) to the region within the red rectangle in Fig. 2a: this region includes most of the spots of intensive fires observed in northern Eurasia during the period considered. The idea behind this limitation is that the selected atmospheric observations should not be affected to a significant extent by emissions from fires or other sources outside of Siberia. Otherwise, our estimates could become more uncertain or biased. For the same reason, the period considered does not include April. Indeed, although there were some (mainly grass) fires in the selected region during that month, very strong fires contributing to air pollution over Siberia in April took place in Kazakhstan; estimation of emissions from those fires is beyond the scope of this study. Note that the optimisation of the fire emissions was not limited to the selected region: they were calculated in the same way throughout the whole model domain (see Sect. 3.2.1).

2.2 Approximation of the diurnal variations of FRP

The knowledge of the diurnal variation of FRP, $h_l(t)$, is needed in order to extrapolate the selected FRP measurements over any moment of each day considered, and to estimate the daily mean FRP density, Φ_d (see Eqs. 1 and 2). Inaccuracies in $h_l(t)$ can result in systematic biases in the total emissions from a considered region, even when the other parameters involved in Eq. (1) are perfectly accurate. As it has been argued in earlier publications (Ichoku et al., 2008; Vermote et al., 2009), four overpasses of the AQUA and TERRA satellites during a day do not usually allow retrieving of the FRP diurnal variation directly from the MODIS measurements. Nonetheless, since the MODIS measurements span several different periods of a day (see Fig. 3a), they still may contain some useful information on parameters of the diurnal cycle of FRP, as was demonstrated by Vermote et al. (2009) who analysed the MODIS FRP data together with the FRP data from geostationary satellites.

Rather than attempting an accurate estimation of the FRP diurnal cycle, here we aim at finding a way to avoid the potential biases in our optimal estimates of α^s by properly "balancing" the contributions from the selected FRP measurements collected by the MODIS sensors at different hours of the day. Note that a daily maximum of FRP from a given fire can be detected during any overpass of a satellite, particularly because observational conditions during other overpasses on the same day can be unfavourable, and also because the actual FRP diurnal cycle is probably irregular and different for different fires. We require that when the balance is correct, any time interval of the selected observations should yield, integrally, the same daily mean FRP densities (Φ_d) (as it would be expected if the measurements were continuous and perfect and the diurnal cycle of FRP in each grid cell was known exactly). Mathematically, the required regional balance is established through minimizing the following cost function, Λ_l:

$$\Lambda_l = \sum_{j=1}^{4}\sum_{k=1}^{4}(1-\delta_{jk})\left[\sum_{i=1}^{N_{jl}}\frac{\Phi_{ij}(t_i)}{h_{al}(t_i)} - \sum_{i=1}^{N_{kl}}\frac{\Phi_{ik}(t_i)}{h_{al}(t_i)}\right]^2, \quad (4)$$

where the indexes j and k designate the time intervals of the Aqua and Terra satellite overpasses (see Fig. 3a), Φ_{ij} and Φ_{ik} are the daily maximum FRP densities in a given grid cell (see explanations for Eq. 2), N_{jl} or N_{kl} are the total numbers (for the considered region and period) of daily maximum FRP observations falling in the given intervals j or k, δ_{jk} is the Kronecker's symbol, and $h_{al}(t)$ is the smooth Gaussian function,

$$h_{al}(t) = \omega_l + (1-\omega_l)\xi_l \exp\left(-\frac{(t-\tau_{0l})^2}{2\sigma_{hl}^2}\right), \quad (5)$$

approximating the regionally-averaged FRP diurnal cycle ($h_l(t) \cong h_{al}(t)$) for a given category l of the land cover (independently of a grid cell). The three independent parameters (σ_{hl}, τ_{0l}, and ω_l) of such an approximation were chosen following Kaiser et al. (2009a) and Vermote et al. (2009), and enable optimizing the width, amplitude and the time of the maximum of the assumed diurnal cycle. Minimization of Λ_l yields optimal estimates of these parameters, while

a value of ξ_l is determined from normalization. Note that although the intervals "2" and "3" (see Fig. 3a) of the respective Aqua and Terra measurements formally coincide, they actually contain somewhat different information on the diurnal cycle, because the overpasses by Terra take place three hours earlier than those by Aqua.

The minimization is performed with the data on the fine resolution grid of $0.2° \times 0.1°$ by means of direct scanning of the parameter space of the approximation; specifically, the parameter values were varied in embedded cycles by a small step within sufficiently wide intervals (for example, σ_{hl} was varied from 0.1 to 10 with a step of 0.01). On the one hand, such a simple method allowed us to avoid the risk of finding a local minimum of the nonlinear cost function instead of a global one (whereas most standard iterative minimization routines might become "trapped" in a local minimum). On the other hand, considerations of computational efficiency were not important in the given case due to relative simplicity of the numerical problem in question. We made sure that the mean relative uncertainty of the optimized diurnal cycle due to finite steps of parameter values in the optimization procedure does not exceed 10 %. The optimization was made independently for fires in forests and in grassland: daily FRP densities for a given cell were taken into account in Eq. (4) only if the fraction of the vegetative land cover of a given type in a given grid cell exceeded 67 %. The approximations of the FRP diurnal cycle obtained for the cases of forest and grassland fires are shown in Fig. 3b. The diurnal variation is rather strong in both cases, even more in the case of forest fires, while its maximum is reached one hour earlier in the case of the grassland fires.

Since the region considered is not covered by FRP measurements of geostationary satellites, any direct comparison of our estimates with similar estimates derived from geostationary measurements is not feasible. Nonetheless, it may be useful to note that by means of Fourier analysis of the FRP data (without selecting their daily maxima) from the SEVIRI geostationary instrument, Sofiev et al. (2013) found that forest fires show a more pronounced diurnal variation than grass fires, similar to our results (although there was no lag in time). The amplitude of the variations was by factors of about 1.25 and 1.5 larger in the estimates by Sofiev et al. (2013) than in our estimates for forest and grass fires, respectively. These differences can, in particular, be due to the fact that the SEVIRI FRP data are dominated by measurements of African tropical fires (which are likely to feature a somewhat different diurnal variation than fires in boreal regions). On the other hand, due to insufficient temporal coverage of the MODIS measurements, our approximation may indeed underestimate the diurnal cycle amplitude. However, as noted above, the main purpose of the diurnal cycle estimation in this study is to establish a proper balance between the contributions of the FRP measurements made to the emission estimates during different periods of the day,

and the optimization procedure described above allowed us to achieve this goal.

2.3 Optimization of the FRP-to-BBR conversion factors

2.3.1 Cost function definition

The optimum values of the FRP-to-BBR conversion factors $\boldsymbol{\alpha}^s$ are obtained by minimizing the cost function, J, depending on the observed ($\mathbf{V}_o$) and simulated ($\mathbf{V}_m$) AOD or CO data provided daily on a model grid:

$$\boldsymbol{\alpha}^s = \arg\min[J(\mathbf{V}_o, \mathbf{V}_m)]. \tag{6}$$

Here, different components of the vector $\boldsymbol{\alpha}$ represent various land cover types and should be optimized simultaneously. As it is common for inverse modelling studies, we assume that random discrepancies between the observations and simulations satisfy the normal distribution. To take into account systematic discrepancies (which are not associated with fire emission uncertainties) between the observations and simulations, we introduce (and then estimate) the bias, $\boldsymbol{\Delta}$, which is supposed to include systematic errors both in the measurements and in the model.

To evaluate this bias (as explained in detail in the next section), we select the days and grid cells in which the contribution of fires to $\mathbf{V}_m$ (and, presumably to $\mathbf{V}_o$, too) is negligible. These grid cells should accordingly be excluded from the cost function in order to avoid interference between the bias and other (random) uncertainties. This is done by means of the operator θ, which is defined as follows:

$$\theta^{ij} = 1 \left| \frac{\left(V_m^{ij} - V_{m(r)}^{ij}\right)}{V_{m(r)}^{ij}} > \varepsilon \right\rangle$$

$$\theta^{ij} = 0 \left| \frac{\left(V_m^{ij} - V_{m(r)}^{ij}\right)}{V_{m(r)}^{ij}} \leq \varepsilon \right\rangle, \; i \in [1, N_c], \; j \in [1, N_d], \tag{7}$$

where $\mathbf{V}_{m(r)}$ are the outputs of the "reference" model run performed without fire emission, i and j are indices of a grid cell and a day, N_c and N_d are the total numbers of the grid cells and days considered for optimisation of $\boldsymbol{\alpha}$, respectively, ε is a small number. Accordingly, we define the cost function as the mean square deviation of the simulated daily values from the observed ones:

$$J = \sum_{j=1}^{N_d} \sum_{i=1}^{N_c} \theta^{ij} (V_m^{ij} - V_o^{ij} - \Delta^{ij})^2. \tag{8}$$

The results presented below (see Sect. 4) are obtained with $\varepsilon = 0.1$, that is, when fire emissions contribute less than 10 % to the simulated data, the corresponding days are excluded.

2.3.2 Bias estimation

The bias, $\boldsymbol{\Delta}$, can be evaluated in different ways depending on the assumptions regarding its nature and origin. In par-

ticular, when the bias is assumed to be predominantly associated with the boundary conditions (as assumed here in the analysis of CO data), we evaluate it as the mean difference between the simulations (without fire emissions) and measurements:

$$\Delta^{ij} = \sum_{j_p} \sum_{i_p} (1 - \theta^{i_p j_p}) \left[V_{\mathrm{m(r)}}^{i_p j_p} - V_{\mathrm{o}}^{i_p j_p} \right] N_p^{-1},$$

$$i_p \in I_p(i),\ j_p \in J_p(j), \tag{9}$$

where I_p and J_p are sufficiently large sets of grid cells and days in a region and a period covering a given grid cell i and a day number j. Our choice for the optimal sizes of I_p and J_p is explained below in this section.

On the other hand, when the bias is likely associated predominantly with errors in the assumed relation between a model output and a measured characteristic and/or biases in local sources of the considered species, we introduce it (as in our analysis of AOD data) by means of a correction factor representing the ratio of the mean measured and simulated (without fire emissions) data:

$$\Delta^{ij} = -V_{\mathrm{m(r)}}^{ij} \left[\frac{\sum_{j_p} \sum_{i_p} (1 - \theta^{i_p j_p}) V_{\mathrm{o}}^{i_p j_p}}{\left(\sum_{i_p} \sum_{j_p} (1 - \theta^{i_p j_p}) V_{\mathrm{m(r)}}^{i_p j_p} \right)} \right],$$

$$i_p \in I_p(i),\ j_p \in J_p(j). \tag{10}$$

The sets I_p and J_p are determined as a trade-off between different kinds of possible uncertainties in the bias estimates. On the one hand, there may be random uncertainties (and moreover, the bias estimation may even become impossible) due to an insufficient amount of data involved in Eq. 9 or 10. On the other hand, there may be a representativeness error (that is, the biases evaluated for too large regions and/or time periods may be not representative of the systematic errors of the simulations on smaller scales). In the application considered in this study, the biases were estimated on a $1° \times 1°$ model grid; the sets I_p included (when available) 40 grid cells symmetrically surrounding a given grid cell in the west-to-east direction and 20 grid cells in the south-to-north direction; the set J_p included (when available) 7 days before and after a given date.

2.3.3 Uncertainty estimation

The uncertainty ranges for our estimates of $\boldsymbol{\alpha}^s$ were evaluated by means of a Monte-Carlo experiment (Press et al., 1992). The Monte Carlo experiment performed in this study was set up to take into account the uncertainties associated with (1) the residual errors in $\mathbf{V}_{\mathrm{m}}$ and $\mathbf{V}_{\mathrm{o}}$ (that is, the differences between $\mathbf{V}_{\mathrm{m}}$ and $\mathbf{V}_{\mathrm{o}}$ remaining after optimization of $\boldsymbol{\alpha}$, see Eq. 8), and (2) the uncertainties in the regional-scale estimates of the emission factors, β_s. Note that apart from model errors in transport and chemical transformation processes, the residual errors in $\mathbf{V}_{\mathrm{m}}$ include uncertainties associated with local deviations of the emission factors from their

regional-scale estimates due to, e.g., different fire regimes (Akagi et al., 2011) and diverse spatial patterns of plant populations in Siberia (Schulze et al., 2012). In the case of $\boldsymbol{\alpha}$ derived from AOD measurements, we additionally took into account the uncertainties associated with the magnitude of the mass extinction efficiency employed to convert the modelled aerosol concentration into AOD (see the corresponding definitions and discussion in Sect. 3.2.3). The experiment included a sufficiently large number (1000) of iterations. The simulated data obtained with the optimized values of $\boldsymbol{\alpha}$ were used as a substitute for the true values of the variable considered. Random uncertainties added in each iteration to the "true" values of a variable were specified by means of the bootstrapping method (Efron et al., 1993) as the randomly shuffled residuals $V_{\mathrm{m}}^{ij} - V_{\mathrm{o}}^{ij} - \Delta^{ij}$ for different grid cells i and days j. The considerable advantage of the bootstrapping method (in comparison to a Monte Carlo experiment based on explicit specification of a probability distribution function) is that it allows avoiding any a priori assumption about the nature of uncertainties in the observed and simulated data. To preserve possible spatial and temporal co-variations between the residual errors in the CO and AOD data, random shuffling of grid cells i and days j in CO and AOD datasets was done in exactly the same order. In each iteration, positive values of the emission factors, β^s, and (in the case of aerosol emissions) of the mass extinction efficiency were sampled from the lognormal distributions representing their uncertainties and used instead of their assumed best values specified (along with the parameters of the corresponding probability distributions) in Sects. 2.4 and 3.2.3. Based on the analysis of the relationship between several currently available experimental estimates of the emission factors for CO and aerosol (see the Supplementary material), we assumed that uncertainties in the emission factors β^s for these different species are independent. The experiment outputs (that is, varying random estimates of $\boldsymbol{\alpha}$) were processed to evaluate the geometric standard deviation of the obtained samples of $\boldsymbol{\alpha}^s$ values. The Shapiro–Wilk test performed for these output values indicated (with a confidence level exceeding 95 %) that the logarithms of the sampled values of $\boldsymbol{\alpha}$ satisfy the normal distribution.

Note that while the residual errors (for a given species) in different grid cells and days are assumed here to be statistically independent, the systematic errors in the emission factors, β^s, for a given land cover type are assumed to perfectly covariate in space and time; that is, these errors are assumed to be the same for any moment and grid cell. The same assumption is made for errors in the mass extinction efficiency. Accordingly, the same random values of these parameters are specified, in each of the iterations, for all grid cells and days. The latter assumption can lead to some overestimation of the estimated uncertainty in $\boldsymbol{\alpha}$. Indeed, the emission factors are likely to vary within our large study region, and a part of their variability is already reflected in the residual errors $\mathbf{V}_{\mathrm{m}} - \mathbf{V}_{\mathrm{o}} - \Delta_{ij}$. The mass extinction efficiency of biomass

burning aerosol is also expected to vary both in space and time, depending on fire regime and aerosol age (Reid et al., 2005). However, since the character of these variations is not known, we prefer (to be on the safe side) to overestimate uncertainties in our estimates of the FRP-to-BBR conversion factors (and thus in our emission estimates) rather than to underestimate them.

2.3.4 Optimization algorithm

Minimization of the cost function J (see Eqs. 6–8) involving outputs of a chemistry-transport model can, in a general case, be a very computationally expensive task. Following Konovalov et al. (2011), we assumed that the effects of chemical nonlinearities on relationships between the concentrations of CO and aerosol over regions with intensive wildfires and the resulting emissions are negligible. This allowed us to obtain the optimal parameter values by means of a simple "twin experiment" method. Specifically, the runs with $\alpha_l = 0$ were followed by runs made independently for each of the considered categories of the vegetative land cover with nonzero initial guess values for α_l. As the initial guess for α_l, we used the estimate $(0.368 \, \mathrm{kg \, MJ^{-1}})$ obtained by Wooster et al. (2005) in an analysis of experimental fires. The difference between the outputs of these runs was used to estimate the partial derivatives of $\mathbf{V}_m$ with respect to α_l (for a given l) and to approximate $\mathbf{V}_m$ as a linear function of α_l.

Since the $\mathbf{V}_m$ involved in the selection criterion given by Eq. (7) depends on α_l, minimizing J cannot be done analytically even after linearizing $\mathbf{V}_m$. Thus we employed an iterative procedure: given some initial guess for α_l^s, we found $\mathbf{V}_m$, $\boldsymbol{\theta}$, $\boldsymbol{\Delta}$ and the optimized values of α_l (corresponding to the above defined $\boldsymbol{\theta}$ and $\boldsymbol{\Delta}$); then the initial guess was replaced with such "conditionally" optimal values α_l and the cycle was repeated. Convergence of this procedure was found to be achieved in 3–5 iterations.

2.4 Estimation of CO_2 emissions

In accordance with the general principles of inverse modelling and Bayesian inference (Tarantola, 1987), we consider the estimate of the FRP-to-biomass rate conversion factor (α_l) inferred from measurements of the species s, as a sample taken from the probability distributions characterizing uncertainties of the estimation procedure. Taking into account that physically acceptable estimates of α_l should be positive, we assume that they satisfy the lognormal probability distribution $f_{\alpha_l}(\alpha_l, \mu_l, \sigma_l)$, where μ_l is assumed to be a logarithm of the true (unknown) value of α_l. Given two estimates of α_l inferred from CO (α_1) and AOD (α_2) measurements with the corresponding (a priori known) error covariances V_{11} $(= \sigma_1^2)$, $V_{12}(= c)$ and $V_{22}(= \sigma_2^2)$, the maximum likelihood estimates of the parameters μ_l and σ_l (denoted below as $\hat{\mu}_l$

and $\hat{\sigma}_l$) can be evaluated as follows:

$$\hat{\mu}_l = \frac{\sigma_1^{-2}(1 - c\sigma_2^{-2})\ln(\alpha_1) + \sigma_2^{-2}(1 - c\sigma_1^{-2})\ln(\alpha_2)}{\sigma_1^{-2} + \sigma_2^{-2} - 2c(\sigma_1\sigma_2)^{-2}}, \quad (11)$$

$$\hat{\sigma}_l^2 = \frac{1 - c^2(\sigma_1\sigma_2)^{-2}}{\sigma_1^{-2} + \sigma_2^{-2} - 2c(\sigma_1\sigma_2)^{-2}}. \quad (12)$$

Values of $\hat{\boldsymbol{\mu}}$ and $\hat{\boldsymbol{\sigma}}$ can then be used to express the combined optimal estimates of $\boldsymbol{\alpha}$ ($\hat{\boldsymbol{\alpha}}$) and its geometric standard deviation ($\hat{\boldsymbol{\sigma}}_{\mathbf{g}}$):

$$\hat{\boldsymbol{\alpha}} = \exp(\hat{\boldsymbol{\mu}}), \quad (13)$$

$$\hat{\boldsymbol{\sigma}}_{\mathbf{g}} = \exp(\hat{\boldsymbol{\sigma}}). \quad (14)$$

It is noteworthy that according to Eq. (12), the uncertainty of the combined estimates of α_l is expected to be always smaller than the uncertainty of the estimates derived from the measurements of only one species. For convenience, the values of α_1, α_2 and $\hat{\alpha}_l$ are denoted below as α_l^{co}, α_l^{aod}, α_l^{cmb}, respectively.

The maximum likelihood estimates of α_l for different types of vegetative land cover can then be used to estimate the CO_2 emission rate, E^{CO_2}, by using Eq. (1):

$$E^{CO_2}(t) = \Phi_d \sum_l \alpha_l^{cmb} \beta_l^{CO_2} \rho_l h_l(t). \quad (15)$$

The uncertainties in E^{CO_2} can be estimated by means of a Monte Carlo experiment in which values of α are sampled (in each iteration) from the lognormal distribution with the parameters defined by Eqs. (13), (14), and the CO_2 emission factors, β^{CO_2}, also varied within their uncertainty range in accordance with the corresponding log-normal probability distribution. The Monte-Carlo experiment performed in this study included 1000 iterations.

Note that due to covariation of errors in α_l^{co} and α_l^{aod} ($c \neq 0$) the uncertainty in α_l^{cmb} can be larger compared to the case when the errors are independent. As a potential source of the error covariation, we attempted to take into account possible common model errors in transport and emissions of CO and aerosol (see Section 2.3.3). However, since the exact nature and characteristics of uncertainties in the input data for our analysis are not known (as it is common for virtually any "real world" application of the inverse modelling approach), the uncertainties reported below for our estimates of the conversion factors and CO_2 emissions should be considered with caution. Taking into account the arguments given in Sect. 2.3.3, we believe that our estimates of uncertainties in α_l^{cmb} (and thus in the estimates of CO_2 emissions) are more likely to be overestimated than underestimated.

Note also that as an alternative to the method outlined above, the CO_2 emission estimates can be derived from measurements of only one species (CO or aerosol). For such a case, the combined optimal estimate in Eq. (15) should be replaced by the estimate (α_l^{co} or α_l^{aod}) based on the measurements of the respective species, and the corresponding

standard deviations (σ_1 or σ_2) should be used for estimation of uncertainties in the framework of the Monte Carlo experiment. The focus is given below (see Section 4) to the CO$_2$ emission estimates based on the combined measurements of two species, since we consider such estimates to be more accurate and reliable than the estimates based on the single-species measurements; however the estimates derived separately from CO and AOD measurements are also presented.

2.5 Emission factors

In the application described here, we employ the CO$_2$ and CO emissions factor estimates and their uncertainties, based on Andreae and Merlet (2001) and subsequent updates (Andreae, M. O., unpublished data, 2013). These estimates have been obtained as a result of the compilation of a large number of dedicated laboratory and field measurements. They are very similar (taking into account the uncertainty range) to the estimates provided by Akagi et al. (2011), as well as to the estimates employed in the GFED3.1 (van der Werf, 2010) and GFASv1.0 (Kaiser et al., 2012) emission inventories. Here, we characterize the range of uncertainties in the emission factors by means of the geometric standard deviation inferred from the variability of the emission factors originally reported in terms of the standard deviation. The assigned emission factors for CO$_2$, CO, OC, and BC along with their uncertainties are presented in Table 1.

The emission factors for nitrogen oxides (NO$_x$) and non-methane hydrocarbons (NMHC) are specified in the same way as in Konovalov et al. (2011) (see Table 2 and references to the sources of the estimates therein). Note that although NO$_x$ and NMHC participate in the chemical processes affecting the evolution of CO and driving the formation of secondary inorganic and organic aerosol, the impact of the atmospheric chemical processes on evolution of pyrogenic CO and aerosol concentrations at the scales considered was found to be very small (in accordance with an assumption mentioned in Sect. 2.3 and test results presented for a similar situation in Konovalov et al. (2011)). For this reason, the uncertainties in the emission factors for NO$_x$ and NMHC are not taken into account.

3 Measurements and simulations of atmospheric composition

3.1 Atmospheric measurement data

3.1.1 CO measurements

To constrain the CO emissions we used measurements from the Infrared Atmospheric Sounding Interferometer (IASI) on board the METOP-A satellite (Clerbaux et al., 2009) in May–September 2012. The CO concentration is retrieved from the measured spectrum at the 1-0 rotation vibration band centred at 4.7 µm (2128 cm^{-1}) by using the Fast Optimal Retrievals on Layers for IASI (FORLI) algorithm (Hurtmans et al., 2012). The sun synchronous orbit (with equator crossing at 09:30 LT for the ascending node) of the METOP-A satellite, and 120 spectra measured along each swath provide global coverage twice a day.

The performance of the IASI CO retrieval in highly polluted conditions associated with intensive wildfires was evaluated by Turquety et al. (2009) for the case of the fires in Greece in 2007. They found that under the prevailing conditions the typical vertical resolution of the CO retrievals was about 8 km. They also found that, although the presence of heavy smoke may cause some underestimation in the retrieval, the contribution of the probable bias to the total retrieval error, which tends to slightly increase in the fresh fire plumes, is relatively small (typically 10 % or less). The usefulness of the IASI CO retrievals as the source of quantitative information on CO fire emissions was later confirmed, in particular, by Kroll et al. (2013) and R'Honi et al. (2013) for the case of the 2010 Russian wildfires.

Similar to Turquety et al. (2009) and Kroll et al. (2013), we used the CO total columns. Although under background conditions, the signal contributing to the retrieval of the total CO columns mostly comes from the upper layers of the troposphere, the contribution of the lower troposphere under certain conditions may be relatively large (George et al., 2009). The possibility to retrieve information about CO in the lower troposphere under given conditions can be characterized by the DOFS (degrees of freedom for signal) parameter which is defined as the trace of the averaging kernel matrix. Detection of CO in the lower troposphere requires DOFS to be about 2 or higher (George et al., 2009). For example, the typical daytime DOFS values in the above-mentioned retrievals over Greek fires were about 1.8 (Turquety et al., 2009). Accordingly, to enhance the fire signature in the CO columns considered here, we have selected retrievals with DOFS > 1.7. This threshold value (which is exceeded in 58 % of the retrievals in the period considered) is a compromise to avoid getting larger uncertainties in our emission estimates due to a smaller contribution of the boundary layer to the CO columns or due to insufficient amount of the selected data (with large DOFS). The sensitivity of the results of this study to the threshold value was examined and found to be small compared to other uncertainties.

In addition to satellite CO measurements, we used the ground based measurements of near-surface CO concentrations at the Zotino Tall Tower Observatory (ZOTTO) site (Schulze et al., 2002; Lloyd et al., 2002; Chi et al., 2013; http://www.zottoproject.org/) situated in central Siberia (89.35° E, 60.80° N). We used the daily mean CO concentrations obtained by averaging the original hourly data. The data collected during the warm period of the year were available for this study only for the years 2007 and 2008 (and with substantial gaps). While the CO measurements were performed simultaneously at two levels of the tower (50 m and 300 m), we found that the differences between them are negligible in

comparison to the differences to the simulations performed in this study. Taking this into account, only the measurements at 50 m were used in our analysis.

3.1.2 Aerosol optical depth (AOD) measurements

As a source of information on the aerosol content in the atmosphere we used satellite retrievals of AOD at 550 nm in May–September 2012. The daily AOD data retrieved from MODIS measurements on-board the AQUA and TERRA satellites were obtained as the L3 MYD08_D3/MOD08_D3 data product from the NASA Giovanni-Interactive Visualization and Analysis system (http://daac.gsfc.nasa.gov/giovanni/). The spatial resolution of the AOD data is $1° \times 1°$. The retrieval algorithm is described in Kaufman et al. (1997) and Remer et al. (2005). The relative uncertainty of the MODIS AOD data over land is estimated to be about 20 % (Ichoku et al., 2005).

3.2 Simulated data

3.2.1 Model configuration

The relationships between the measured CO columns or AOD and the corresponding biomass burning emissions were simulated by means of the CHIMERE chemistry-transport model (www.lmd.polytechnique.fr/chimere). CHIMERE is a typical mesoscale Eulerian three-dimensional model that is designed to simulate the evolution of the chemical composition of the air in the boundary layer and the lower troposphere. The parameterizations of the different physical and chemical processes that are taken into account in the model are described in several papers (e.g., Schmidt et al., 2001; Bessagnet et al., 2004, 2009; Menut et al., 2013). The modifications introduced in the standard version of the model in order to take into account the effects associated with wildfires are described in Konovalov et al. (2011; 2012).

The simulations were performed with a horizontal resolution of $1° \times 1°$ for 12 layers in the vertical (up to the 200 hPa pressure level). The main model domain (35.5–136.5° E; 38.5–75.5° N) covered a major part of Northern Eurasia, including Siberia and parts of Eastern Europe and the far east (see Fig. 1). Note that the inclusion of a part of European Russia allowed us to take into account anthropogenic emissions from the major Russian industrial regions. In addition, we used the nested domain (86.2–92.4° E; 57.6–63.9° N) covering a central part of Siberia with a higher resolution of $0.2° \times 0.1°$ to simulate the evolution of the near surface CO concentration at the ZOTTO site. Meteorological data were obtained from the WRF-ARW model (Skamarock et al., 2005), which was run with a horizontal resolution of 90 km × 90 km and driven with the NCEP Reanalysis-2 data. Chemical processes were simulated with the simplified MELCHIOR2 chemical mechanism (Schmidt et al., 2001) with recent updates. The main model runs were performed

for the period from 18 April to 30 September 2012 by using the initial and boundary conditions for gases and aerosols from climatological runs of the MOZART (Horowitz et al., 2003) and GOCART (Ginoux et al., 2001) models, respectively. Additionally, the simulations were done for the periods covered by CO measurements at the ZOTTO site in 2007 and 2008. Anthropogenic emissions were specified using the EDGAR version 4.2 data (EC-JCR/PBL, 2010), and biogenic emissions were calculated "online" by using biogenic emission potentials from the MEGAN global inventory (Guenther et al., 2012).

Aerosol was simulated by using 8 size bins with diameters ranging from 10 nm to 10 μm. Both dry deposition of aerosol particles and their scavenging by clouds and precipitation were taken into account. Primary aerosol particles emitted from fires were assumed to consist of only carbonaceous material, with a distinction made between organic carbon (OC) and black carbon (BC). Secondary organic aerosol (SOA) formation was parameterized by using the single-step oxidation method (Pun et al., 2006) introduced in CHIMERE as described by Bessagnet et al. (2009). Evolution of secondary inorganic aerosol was computed with the tabulated version of the thermodynamic model ISORROPIA (Nenes et al., 1998). Dust aerosol emissions were taken into account by means of the simple method described by Vautard et al. (2005). The simulated aerosol concentration was used to estimate the AOD as described in Sect. 3.2.3.

3.2.2 Approximation of the injection height of pyrogenic emissions

The maximum injection height of air pollutant emissions is commonly regarded as one of the important parameters determining the atmospheric fate of biomass burning emissions, and several different ways to estimate this parameter have been suggested (see, e.g., Sofiev et al., 2012, 2013 and references therein). Here, we used the parameterization proposed recently by Sofiev et al. (2012). The advantage of this parameterization in the context of this study is that it is designed directly for use with FRP data from the MODIS measurements. Specifically, Sofiev et al. (2012) proposed to estimate the maximum injection height (or, in other words, the maximum plume height, H_p) as follows:

$$H_p = \alpha H_{abl} + \beta \left(\frac{FRP}{P_{f0}} \right)^\gamma \exp\left(-\frac{\delta N_{FT}^2}{N_o^2} \right), \qquad (16)$$

where H_{abl} is the unperturbed boundary layer height, N_{FT} is the Brunt–Väisälä frequency in the free troposphere, P_{f0} and N_o are normalization constants ($P_{f0} = 106$ W, $N_o^2 = 2.5 \times 10^{-4}$ s^{-2}) and α, β, δ, and γ are the fitting parameters ($\alpha = 0.24$; $\beta = 170$ m; $\delta = 0.35$; $\gamma = 0.6$). Sofiev et al. (2012) demonstrated that this parameterization is superior to some alternative parameterizations of H_p, although a considerable part of the variability of the measured H_p still remained un-

explained by Eq. (16) (partly due to large uncertainties in the FRP and H_p measurements).

In this study, H_p was estimated for each fire pixel at the moment of a measurement, and the estimates are extended to the whole day by using the approximated diurnal variation, $h_{al}(t)$, of FRP. The hourly injection profiles for the pixels falling into a given grid cell of $0.2° \times 0.1°$ or $1° \times 1°$ were averaged with weights proportional to the measured FRP values. The emissions calculated using Eq. (1) for each hour were distributed uniformly from the ground up to the height determined by the respective hourly value of H_p.

To test the sensitivity of the results of this study to the possible uncertainties in the estimated maximum injection height, we additionally employed a simpler approximation assuming that H_p is a constant parameter equal to 1 km. Such a highly simplified estimation of the actual injection height is partly based on the analysis presented by Sofiev et al. (2009), and yielded reasonable results in Konovalov et al. (2011). Actually, the difference between simulations performed with different approximations of the maximum injection height can be expected to be small, except in relatively rare cases, when H_p strongly exceeds the daily maximum of the boundary layer height. Otherwise, irrespective of the actual H_p value, the emissions are likely to be distributed throughout the boundary layer due to fast turbulent mixing. Our results presented in Sect. 4 confirm this expectation.

3.2.3 Processing of model outputs

As described by Fortems-Cheiney (2009), in order to properly compare a vector of atmospheric model outputs, x_m (where the components are partial columns at different levels), with IASI retrievals for a given grid cell, the simulated data should be transformed with the corresponding averaging kernel matrix, $\mathbf{A}$:

$$x_{mt} = \mathbf{A}(x_m - x_a) + x_a, \tag{17}$$

where x_{mt} are the transformed model outputs and x_a is the a priori CO profile used in the retrieval procedure. The missing components of x_m for the altitudes exceeding the altitude of the upper layer of CHIMERE are taken to be equal to the corresponding values from x_a. The transformation given by Eq. (17) was performed independently for each pixel containing measurements satisfying the general selection criterion (see Sect. 3.1.1). Values of x_{mt} were vertically integrated to obtain the total CO columns. Since the horizontal spatial resolution of the IASI data is higher than that of our model outputs, the same model profile in a given grid cell was used with different averaging kernels. CO column values available for the same grid cell and day were averaged.

To obtain AOD values from model outputs, we followed a simple and robust approach described by Ichoku and Kaufman (2005). Specifically, the AOD value, τ_m, was derived from the simulated aerosol mass column concentration, M_a, as follows:

$$\tau_m = M_a \sigma_e, \tag{18}$$

where σ_e is the mass extinction efficiency, which is the sum of the mass absorption and mass scattering efficiencies. Similar to Ichoku and Kaufman (2005), we select a typical value of σ_e from measurement data collected in several experimental studies of optical properties of biomass burning aerosol (Reid et al., 2005). After having averaged the data corresponding to the 550 nm wavelength from the experiments that provided both the mass absorption and mass scattering efficiencies along with their variability (but excluding the data collected in tropical forests), we estimated the mean value of σ_e to be $4.7\,\mathrm{m^2\,g^{-1}}$. This value is very similar to that ($4.6\,\mathrm{m^2\,g^{-1}}$) chosen by Ichoku and Kaufman (2005) in their study to characterize the mass extinction efficiency of biomass burning aerosol at a global scale. Similarly, after having averaged the variability ranges reported in Reid et al. (2005) for the selected experiments, we estimated the typical standard deviation of σ_e to be of $\pm 0.8\,\mathrm{m^2\,g^{-1}}$. In our Monte-Carlo experiments aimed at estimating uncertainties in the FRP-to-BBR conversion factors (see Sect. 2.3), random values characterizing the variability in σ_e were sampled from the corresponding lognormal distribution with a geometric standard deviation of 1.19.

3.2.4 Model run settings

The base model runs (referred below to as the "Fires_base" runs), which were expected to provide the best estimates of the FRP-to-BBR conversion factors and CO$_2$ emissions from wildfires, were performed by taking into account fire emissions with the estimated diurnal variation (see Sect. 2.2) and by using the advanced parameterization of the emission injection height (see Eq. 16). To examine the sensitivity of our results to possible uncertainties in the injection height and the diurnal variation of fire emissions, we performed two additional simulations. Specifically, the "Fires_test1" model runs were made with the same model configuration as the "Fires_base" runs, but with a constant maximum injection height of 1 km (see Sect. 3.2.2). The "Fires_test2" model runs are also the same as the "Fires_base" runs, except that they were performed with a constant diurnal profile ($h_{al} = 1$) for the fire emissions. Additionally, a reference model run ("No_fires") was made without any emissions from wildfires. All the simulations had the same boundary conditions.

4 Results

4.1 FRP-to-BBR conversion factors and CO$_2$ emissions: optimal estimates for Siberian fires in 2012

Our estimates of the FRP-to-BBR conversion factors, α, for forest and grass fires are reported in Table 2, and the estimates of the total CO$_2$ emissions from fires in the region

considered (see Fig. 2a) are given in Table 3. The estimates were obtained after withholding the CO and AOD data for each third day (the days were counted from the initial day of our simulations, 18 April) for validation purposes. The estimates are reported for three cases with different simulation settings (see Sect. 3.2.4). Different estimates of α inferred from the measurements of CO (α^{co}) and AOD (α^{aod}) were combined as explained in Sect. 2.4 by taking into account their uncertainties evaluated in the Monte Carlo experiments. Note that the covariance of errors in α_l^{co} and α_l^{aod} was found to be very small ($R^2 < 0.01$) in all of the cases considered and did not affect significantly the combined estimates of α (α^{cmb}). The total CO_2 emission estimates reported in Table 3 are obtained by using either α^{cmb}, or α^{co} and α^{aod} taken independently. If not specified otherwise, the CO_2 emissions estimates discussed below are based on α^{cmb}, that is, on both the CO and AOD measurements.

One of the noteworthy results of our analysis is that the differences between α_l^{co} and α_l^{aod} are not statistically significant (for all of the cases), as the indicated ranges of their uncertainty overlap (see Table 2). This result supports the adequacy of our estimates of uncertainties in the conversion factors and, therefore, the feasibility of the probabilistic combination of α^{co} and α^{aod}. However, it should be mentioned that if the difference between α_l^{co} and α_l^{aod} exceeded their combined uncertainty range (for any l), this would not necessarily mean that α^{co} and α^{aod} were inconsistent; formally, it would indicate only that the probability of a type I error (in our case, this is the error of rejecting the hypothesis about the equality of the mathematical expectations of α^{co} and α^{aod}) is relatively small (less than 32 percent in our case).

Note that the uncertainties in our estimates of the FRP-to-BBR conversion factors do not appear to be unusually large in view of the numerous cases of comparable uncertainties in the different available pyrogenic CO and aerosol emission estimates. For example, Huijnen et al. (2012) reported a very large difference (by a factor of 3.8) between the GFED3.1 and GFASv1.0 CO emission estimates (3.6 and 13.8 TgCO, respectively) for the mega fire event in Western Russia in summer 2010; an even larger estimate (~ 20 TgCO) was obtained for a similar region and period by Krol et al. (2013). Petrenko et al. (2012) found that a global model driven by different bottom-up fire emission inventories systematically underestimates AOD over Siberia by up to a factor of 3, but (at least with some of the inventories considered) strongly overestimates it, also by up to a factor of 3, over the equatorial African region. Kaiser et al. (2012) found that in order to match the global patterns of the observations and simulations (based on the GFASv1.0 inventory data) of AOD, the emissions of organic matter and black carbon had to be increased by a factor 3.4 (with respect to emissions of other species). However, this increase resulted in more pronounced fire peaks of AOD in their simulations over boreal regions (including Siberia and the Russian far east) than in the corresponding observations. Therefore, such a big correc-

tion might not really be necessary if simulated and observed AOD were compared only for the region considered in this study. In contrast, Konovalov et al. (2011) found that their CO and PM_{10} simulations were not consistent with the measurements of nearsurface concentrations in the Moscow region in 2010, unless the ratio of CO to PM_{10} emissions from fires was enhanced by about a factor of two with respect to the "standard" settings assuming that the FRP-to-BBR conversion factors for these species are the same.

Qualitatively similar to the results of Kaiser et al. (2012) and Huijnen et al. (2012), we found here (see Table 2) that α_l^{aod} are larger than α_l^{co} by factors of 2.2 and 2.8 in the cases of forest and grass fires, respectively. The uncertainties are found to be considerably larger in α^{aod} than in α^{co}. The fact that the differences between α^{aod} and α^{co} are not statistically significant in our case (as noted above) indicates that they might be explained by uncertainties in emission factors and model errors. Since such uncertainties and errors have already been taken into account (under certain assumptions) in our CO_2 emission estimation procedure, we do not see any sufficient objective reason for totally disregarding the information provided by the AOD measurements, which "automatically" gets a smaller weight in our estimation procedure than the information derived from CO measurements. Even if the actual evolution of biomass burning aerosol were much more complex than it is assumed in our model, the complexity of the atmospheric aerosol processes would likely be manifested as irregular (both in time and space) deviations of our simulations from the measurements, rather than as a uniform difference between them; such irregular deviations have already been taken into account in our uncertainty estimates. Nonetheless, as a caveat, it should be noted that our inverse modelling analysis does not allow us to definitively rule out a contribution of possible additional systematic errors in either the simulated or measured AOD data (apart from the systematic errors reflected in the bias estimates, see Section 2.3.2). Definitive elimination of such potential systematic errors is hardly possible, in particular, without major progress in the current understanding of organic aerosol production processes (see, e.g., Robinson et al., 2007).

Another noteworthy result of our analysis is that our combined optimal estimates of the FRP-to-BBR conversion factors for both forest and grassland fires (see Table 2) are consistent (within the range of their uncertainties) with the local estimate ($\alpha = 0.368 \pm 0.015$ kg MJ^{-1}) obtained from the analysis of experimental fires (Wooster et al., 2005). This result confirms that the FRP daily maxima derived from MODIS measurements are sufficiently representative of the actual FRP (in spite of the fact that some fires can be obscured by tree crowns, clouds and heavy smog). The uncertainties in the estimates of α_l^{co} and α_l^{aod} for grass fires are much larger than in the estimates for forest fires; this is consistent with the fact that the observed signal from forest fires in our study was typically much larger than that from grass fires (see Fig. 2b).

It should be stressed that our analysis does not allow us to make a perfect distinction between forest fires and grass fires: we try to distinguish between them only by considering the relative fractions of forest and grassland in a given grid cell with a fire (see Sect. 2.2). In particular, we cannot distinguish between the emissions coming from the burning of tree crowns (crown fires) or of herbs and debris underneath the forest canopy (ground fires). Note also that our estimates of the FRP-to-BBR conversion factors are only applicable to the Siberian region considered here. Indeed, the relationship between the fire radiative energy detected from space and the amount of biomass burnt may depend on the distribution of burning trees species and the relative prevalence of ground and crown fires. For example, ground fires are probably more wide spread in eastern Siberia, where one of the most abundant tree species is larch (*Larix*), which features fire-resistant properties (Schulze et al., 2012), than in Alaska, where the forest is dominated by spruce (*Picea*) and fir (*Abies*), which have branches located close to the ground (so that a fire can readily climb into the crowns).

The results of the test case "Fires_test1" (see Table 2) indicate that our estimates of α (as well as the estimates of the total CO$_2$ emissions) are rather insensitive to the assumptions regarding the maximum injection height. This result is not surprising since we deal with integral characteristics of CO and aerosol (such as CO columns and AOD); the evolution of these characteristics is likely to be less sensitive to the vertical distribution of the pollutants than, e.g., their concentrations at a certain level. Another probable reason for the small difference between the estimates obtained in the "Fires_base" and "Fires_test1" cases is that the majority (98.7 %) of the hourly injection height values calculated in accordance with Eq. (16) in this study are found to be less than the corresponding daily maxima of the boundary layer height. That is, the emissions were likely to be quasi-uniformly distributed mainly inside of the boundary layer almost irrespectively of the concrete value of the maximum injection height.

In contrast, the simulations performed without the diurnal variation of emissions (see the results for the "Fires_test2" case in Tables 2 and 3) yielded considerably different estimates of α. Specifically, α_l^{co} and α_l^{aod} for forest fires increased by factors of 1.7 and 1.3, respectively. Smaller changes were found in α_l^{co} and α_l^{aod} for grass fires. The interpretation of these changes is rather difficult, since the effect of the perturbations in the diurnal variation of FRP on the estimates of the FRP-to-BBR conversion factors depends on the temporal distribution (sampling frequency) of the selected FRP measurements relative to the perturbations in the diurnal cycle. In general, since the relative differences between the diurnal cycles assumed in the two discussed cases are much larger during night-time than in daytime, the daily mean FRP values estimated with the "flat" diurnal cycle can be expected to be negatively biased, leading to the positive bias in the optimized values of α_l (as it happened in the case

of forest fires). The considerable differences in optimal estimates of α_l for forest fires between the "Fires_base" and "Fires_test2" cases are in line with the discussion in Konovalov et al. (2011), where it was noted that application of the diurnal cycle of emissions with a very strong daytime maximum for estimating daily mean FRP densities resulted in a much smaller optimum values of the FRP-to-BBR conversion factors, compared to the case with a "flat" diurnal cycle of FRP. These differences emphasize the importance of the proper specification of the diurnal variation of emissions in the framework of our method, especially when the estimation of the FRP-to-BBR conversion factors is of interest. However, the biases in the optimized values of α_l can, in principle, be compensated by an increase in the fraction of daytime measurements among the selected daily maximum values, as it, apparently, happened in the case of grass fires.

It is noteworthy that in spite of the rather significant differences between the estimates of α corresponding to the "Fires_base" and "Fires_test2" cases, the consistency between the α^{co} and α^{aod} estimates was retained. And it is especially important, that the estimates of the total CO$_2$ emissions (which are the main goal of this study) obtained in "Fires_test2" are changed rather insignificantly (within the estimated uncertainty ranges) relative to those obtained in the base case (see Table 3). This result reflects, in particular, the small sensitivity of our simulations of daily values of the CO columns and AOD to diurnal variations of the CO or aerosol emissions (when the daily mean FRP values are kept unchanged) and is consistent with similar results by Krol et al. (2013). On the whole, the results of the test cases prove that our estimates of CO$_2$ emissions from fires are robust with respect to the simulation settings.

The differences between the CO$_2$ emission estimates (see Table 3) derived from the combination of CO and AOD measurements and from only CO or AOD measurements follow the differences between α^{cmb}, α^{co}, and α^{aod}. Specifically, the total CO$_2$ emission estimates based on the combined CO and AOD measurements are much closer (although about 30 percent higher) to the CO-based estimate than to the AOD-based estimate. The CO-based CO$_2$ emission estimate is much less uncertain than the AOD-based estimate, but more uncertain than the estimate based on the combined CO and AOD measurements. In view of the above discussion concerning the large differences between α^{co} and α^{aod}, our CO$_2$ emission estimates based on CO measurements only can be considered as a more robust ("conservative") alternative to the estimates involving inversion of the AOD measurements only.

The spatial distributions of the optimized CO$_2$ emissions from fires in forests and grasslands in 2012 are shown in Fig. 4. The forest fires were most intense within a rather narrow latitudinal band ($\sim$ 58–63° N) in the western and central part of Siberia and in the far east, while the grass fires (including agricultural fires) were predominant in the Siberian region neighbouring Kazakhstan. The total CO$_2$ emissions

from fires in the study region ($\sim 392\,\mathrm{Tg\,C}$) are comparable to the estimated total annual anthropogenic CO$_2$ emissions in Russia ($\sim 490\,\mathrm{Tg\,C}$ in 2011, according to EDGAR (EC-JRC/PBL, 2011)).

Along with identifying the uncertainties in our results as discussed above, we have carefully examined possible uncertainties associated with the options chosen in our estimation algorithm. Specifically, we varied the value of the parameter ε (see Eq. 7) within a reasonable range (from 0.05 to 0.2). We also "swapped" the ways to estimate the model bias in the cases of estimations based on CO and AOD measurements (see Eqs. 9 and 10) in order to test if our results are sensitive to the assumptions regarding the character (additive or multiplicative) of the bias. Finally, we examined whether our estimates are sufficiently robust with respect to specific definitions of the sets, I_p and J_p, of grid cells and days selected to estimate the bias: specifically, the sets I_p and J_p were increased two-fold in each direction relative to the basic options specified in Sect. 2.3. In all of these cases, the changes in our estimates of the FRP-to-BBR conversion factors and total CO$_2$ emissions were found to be much smaller than the uncertainty ranges reported in Tables 2 and 3 for the base case. Therefore, the sensitivity analysis confirmed that the results of this study are sufficiently robust with respect to the options of the estimation algorithm and the settings of the numerical experiments.

4.2 Validation of the optimal estimates of the FRP-to-BBR conversion factors

If the optimized estimates of the fire emissions are adequate, they can be expected to produce a reasonable agreement of measurements of atmospheric composition over regions affected by fires with the corresponding measurements. Here we present our simulations of CO and aerosol that were performed with the optimized values of α^{co} and α^{aod}, respectively, in comparison with corresponding observations withheld from the dataset used for the optimisation. Spatial distributions of the measured and simulated CO columns averaged over the period from 1 May to 30 September 2012 are shown in Fig. 5. In addition, this figure shows the spatial distributions of CO columns for a selected day (22 July 2012) featuring very strong perturbations of atmospheric composition over Central Siberia. The corresponding distributions of AOD are presented in Fig. 6. The simulated quantities in Figs. 5 and 6 are shown after correcting the bias, as explained in Sect. 2.3. It can be seen that the distribution of the observed mean CO columns is reproduced by the model quite adequately; both the locations of maxima (caused by either fire emissions or anthropogenic sources, as those in northeast China) and their magnitudes in the observations and simulations are very similar. As could be expected, the differences in the daily CO columns from measurements and simulations are somewhat larger, but these differences may, at least partly, be due to uncertainties in the simulated transport processes and are not indicative of any major flaws in the CO emission data. The agreement between the simulated and observed AOD distribution is, in general, also rather good (Fig. 6), although AOD is slightly underestimated in the simulations. The underestimation ($\sim 11\,\%$ on average) is much smaller than the estimated uncertainties in α^{aod}.

The time series of daily values of CO columns and AOD averaged over the study region are presented in Fig. 7. Overall, the model (in the base configuration) reproduces both the CO and AOD measurements rather adequately, although not ideally: specifically, the correlation coefficient, r, exceeds (as in the case of CO columns) a value of 0.9 or (as in the case of AOD) a value of 0.8. The root mean square error (RMSE) of CO columns and AOD does not exceed 5 % and 30 % relative to the corresponding mean values, respectively. The simulations underestimate AOD during the major fire event in July and early August (in western Siberia), but overestimate it in May (the corresponding fires took place mainly in southeastern Siberia). These discrepancies may reflect the fact that emission factors for (especially) aerosol are likely to vary in space and time even across ecosystems of a similar type (e.g., they may presumably depend on fuel moisture). The larger discrepancies between the simulated and measured values of AOD (compared to the case of CO columns) lead to the larger estimated uncertainties in α^{aod} in comparison to the uncertainties in α^{co} (see Table 2). The overall adequacy of the calculated fire emissions is further confirmed by the fact that inclusion of fire emissions into the model enables the reduction of RMSE by a factor of about 2 (relative to the simulation without fire emissions) in both cases.

As it is shown in Fig. 7, the simulations of both CO columns and AOD feature rather considerable biases (which were subtracted in our estimation procedure). The origin of these biases cannot be clearly elucidated in the framework of this study. In the case of the CO columns, one of the major possible factors contributing to the bias in simulations is probably a systematic underestimation of monthly average climatological lateral and top boundary conditions, taken in this study from outputs of the global MOZART model. Earlier, a negative systematic difference between the MOZART outputs and satellite observations for Europe was identified by Pfister et al. (2004). If such a bias was due to underestimation of CO emissions in Europe or on the global scale, it might also be present in the MOZART data for Siberia. The bias in AOD is probably caused by several major factors. First, the bias may reflect a contribution of aerosol from outside of the model domain. Second, it may be due to a probable underestimation of biogenic (secondary) organic aerosol concentration by the CHIMERE model (Bessagnet, 2009). Third, the mass extinction efficiency of the "background" (with respect to biomass smoke) aerosol concentration is likely very different from that of pyrogenic aerosol (Kinne et al., 2003).

It is more difficult to explain, why the bias in the CO columns is larger in July and August than in the other months

(see Fig. 7). On the one hand, such seasonal enhancement of the bias may reflect a mismatch between the locations of CO columns perturbed by fires in observations and simulations. In other words, the "background" CO columns selected from the model outputs may, in some cases, correspond to observed CO columns that are strongly affected by fires. However, this explanation, which can indeed explain some minor short term fluctuations in the bias, does not fit to the fact that the bias enhancement persists for about 15 days even after 14 August (day 105 after 1 May), when the fires and associated perturbations in the simulated CO columns and AOD have almost disappeared (cf. Figs. 2b and 7b with Fig. 7a). On the other hand, the bias enhancement may reflect CO emissions from fires that have not been detected from space (such as fires obscured by clouds or peat fires). However, it is then not clear why those fires are not manifested in a similar way in the bias of the AOD simulations. Similarly, if the model underestimated the influx of CO into the free troposphere, the effect of such underestimation would likely (although not always necessarily) be visible also in the simulated AOD evolution.

Thus, our most probable explanation for the CO bias enhancement is that evolution of CO accumulated during the fire season in the real free troposphere (and, possibly, also in the lower stratosphere) is not properly reproduced in the simulations: the model apparently underestimates the CO residence time in the free troposphere, presumably due to effects of constant monthly average boundary conditions. A part of the discrepancies between simulations and observations may also be caused by transport of CO into the free troposphere over Siberia from outside of the model domain. Anyway, even if the CO bias enhancement really reflects some CO amount residing in the free troposphere but somehow "missed" in our estimation of the CO emissions, this amount can hardly constitute more than 10 % of the total CO amount emitted during the study period in Siberia, as can be inferred from a rough consideration of the CO balance under the assumption that the CO residence time in the free troposphere (in the study period and region) was about 15 days.

A critical test (especially in view of the above discussion) for the optimized fire emissions can be provided by comparison of our simulations with totally independent measurements, such as the measurements of near surface concentrations of CO at the ZOTTO site (see Fig. 8). The simulations for the years 2007 and 2008 were performed with the optimized FRP-to-BBR conversion factors (α^{co} and α^{aod}) from 2012. It can be seen that the measured daily variability is, in general, reproduced by the model rather realistically. It is especially important that the relative difference between the mean (over the two years) CO concentrations in the simulations (after subtraction of the bias) and measurements is rather small ($< 5\%$) and thus provides no indication of a significant bias in CO emissions optimized by means of the satellite CO measurements.

4.3 Comparison of top-down CO_2 emission estimates with inventory data

Figure 9 shows our annual estimates of the total CO_2 emissions from biomass burning in Siberia (in the selected region indicated in Fig. 2a) in comparison to corresponding estimates obtained with the data from the GFASv1.0 (Kaiser et al., 2012) and GFED3.1 (van der Werf et al., 2010) global biomass burning emission inventories. Our estimates were obtained for several years (2007–2012) by using the FRP-to-BBR conversion factors optimized with the data for the period from 1 May to 30 September 2012 and applied to the period from April to September of each year. The gridded CO_2 emission data from the GFASv1.0 and GFED3.1 inventories were integrated over the same region and period as our emission estimates. Unfortunately, the GFED3.1 data for 2012 were not available for this study in view of the expected release of the GFED4.0 inventory. Note that although the GFASv1.0 and GFED3.1 inventories are based on different kinds of input data (specifically, GFASv1.0 is derived from FRP measurements, while GFED3.1 is based on the burnt area data), they are not completely independent. Specifically, the FRP-to-BBR conversion factors in the GFASv1.0 inventory were calibrated with linear regressions against GFED3.1 monthly totals; the calibration was done independently for several categories of land cover including the "extratropical forest with organic soil" land cover class representing mostly the boreal forest regions. Note also that there are major differences in the algorithms used in this study and in the GFASv1.0 inventory to process FRP measurements. In particular, whereas we deal with the daily maxima and estimated diurnal variation of the FRP density as explained in Sect. 2.1, GFASv1.0 processes all measurements available during a given day and estimates the FRP densities at any moment by assimilating earlier FRP measurements (see Kaiser et al., 2012 for details).

As can be seen in Fig. 9, our estimates are systematically larger by at least 30 % than the estimates given by the GFASv1.0 and GFED3.1 inventories, although the difference between the estimates for some years is at the edge of the range of uncertainty in our estimates. Note that the uncertainty range is given in terms of the geometric standard deviation (see Table 3) and represents the 68.3 % confidence level. As it is mentioned in Sect. 2.3, this uncertainty range may be overestimated in our algorithm; in other words, the indicated uncertainties are likely to correspond to a higher confidence level. Our estimate of the total CO_2 emissions in 2012 (392 Tg C with an uncertainty range from 280 to 550 Tg C) is significantly larger (by 73 %) than the corresponding estimate from the GFASv1.0 inventory (226 Tg C). The total emissions in the period from 2007 to 2011 in our estimates (712 Tg C) are larger than the corresponding estimates from GFASv1.0 (383 Tg C) and GFED3.1 (288 Tg C) by factors of 1.8 and 2.5, respectively.

The inter-annual variability is very similar in all the estimates (except for the difference between the data for 2009 and 2010 which is positive in our estimates but is slightly negative in the GFASv1.0 and GFED3.1 data); this fact can be considered as evidence that the FRP-to-BBR conversion factors estimated for fires in the year 2012 are representative of fires in other years as well. Exceptionally large relative differences exist between our estimates and the inventory data for 2010. Specifically, our estimates are by factors of about 2 and 6 larger than the GFASv1.0 and GFED3.1 estimates, respectively. The reason for such large differences is not known, but it may be worth mentioning that several studies (e.g. Fokeeva et al., 2011; Konovalov et al., 2011; Huijnen et al., 2012; Krol et al., 2013) argued that GFED3.1 strongly underestimated CO emissions from the intense wildfires in Russia in 2010. Understanding the large discrepancies between the different emission estimates for the 2010 Russian fires calls for further analysis, which is beyond the scope of this study.

The rather striking similarity between the total CO_2 emission estimates provided by the GFASv1.0 and GFED3.1 inventories can be explained by the above-mentioned calibration of the FRP-to-BBR conversion in the GFASv1.0 inventory by using the data of the GFED3.1 inventory. In spite of this calibration, the spatial distributions of the CO_2 emission fields calculated in the two inventories can be regarded as being sufficiently independent from each other.

The intercomparison of the spatial distributions of the CO_2 emission estimates obtained in this study and calculated with the GFASv1.0 and GFED3.1 inventory data for the year 2008 is illustrated in Figs. 10 and 11. While all the distributions (see Fig. 10) look, in general, rather similar, there are considerable irregular differences not only in magnitudes but also in the locations of fires. In particular, many grid cells exhibit noticeable emissions according to the GFASv1.0 data and our estimates, but are assigned zero or near-zero values in the GFED3.1 inventory. This observation may be considered as an indication of a higher sensitivity of the FRP measurements to actual fire activity, compared to burnt area measurements. However, the differences between our estimates and the GFASv1.0 data are also rather large, probably due to differences in the data processing algorithms.

The scatter plots of the different gridded emission estimates (see Fig. 11) show that the differences between the emissions attributed to a given grid cell in the different inventories frequently reach several orders of magnitude (note that only grid cells with emissions larger than $10^{-4}\,\mathrm{g\,CO_2\,m^{-2}}$ are depicted in the plots and reflected in the statistics). Along with irregular discrepancies between the estimates, there are also some differences that have a systematic character (apart from the differences in the mean values). In particular, grid cells with relatively small emissions (less than $1\,\mathrm{g\,CO_2\,m^{-2}}$) in our data are typically assigned (relatively) much larger values in the GFASv1.0 inventory. This is, likely, a result of the application of the data assimilation procedure, which in the GFASv1.0 inventory efficiently smoothes out strong temporal variations in the FRP densities. This kind of systematic difference between our estimates and the GFASv1.0 data is scarcely visible when these estimates are compared with the data of the GFED3.1 inventory: both the GFASv1.0 inventory and our method yield systematically larger values for the grid cells in which CO_2 emissions evaluated by the GFED3.1 are less than about $1\,\mathrm{g\,CO_2\,m^{-2}}$. This fact is in line with the above remark about a possibly stronger sensitivity of FRP measurements to fire activity, compared to the burnt area measurements.

In spite of substantial "random" differences between these estimates, there are also considerable correlations between the emission fields. Rather surprisingly, correlation of our estimates with the GFED3.1 data ($r \sim 0.71$) is larger than with the GFASv1.0 data ($r \sim 0.66$). This shows that the differences in the data processing algorithms in the situation considered here are at least as important as the differences associated with the different nature of input data. The correlation between the GFASv1.0 and GFED3.1 data is weakest ($r \sim 0.64$). The strong correlation of our data with both these independent datasets suggests that our estimates quite robust and indicates that the overall uncertainties in the spatial distribution of our CO_2 emission estimates are, at least, not larger than the overall uncertainties in the spatial distributions of the GFED3.1 and GFASv1.0 data for Siberia.

5 Summary and conclusions

This paper presents a general method for the estimation of CO_2 emissions from open biomass burning by using satellite measurements. Effectively, the method is based on (1) deriving emissions of some trace species (gases or aerosols) co-emitted with CO_2 by inverting their observations with a chemistry-transport model and (2) rescaling the emissions of those species to the CO_2 emissions by using literature data for emission factors. Using satellite measurements of two (or more) different species in the framework of the proposed method enables cross-validation of the emission parameters inferred from observations of the different species and constraining of uncertainties in the optimal CO_2 emission estimates.

As a source of initial information on the spatial structure and temporal variations of the biomass burning rate (BBR) and pyrogenic emissions, the method employs satellite measurements of the Fire Radiative Power (FRP). Satellite measurements of atmospheric composition are used for optimization of the FRP-to-BBR conversion factors. Applying typical CO_2 emission factors to BBR calculated with the optimized conversion factors yields CO_2 emission estimates indirectly constrained by satellite measurements of co-emitted species.

In this study, the method was applied to the estimation of CO_2 emissions from wildfires in Siberia, which is one of the most important world regions contributing to the global

carbon balance. Optimal values of the FRP-to-BBR conversion factors for boreal forest and grassland fires were independently inferred from the IASI measurements of total CO columns and the MODIS measurements of the aerosol optical depth (AOD) in the warm season of 2012 by using the CHIMERE chemistry-transport model. The spatiotemporal fields of FRP were obtained from the respective MODIS measurements. The diurnal variations of FRP were evaluated by using the same FRP data consistently with estimates of the daily mean FRP values involved in our parameterization of the CO$_2$ emission rates. Note that the emission factors for aerosol, CO and CO$_2$ employed in our analysis were not evaluated in this study, but taken from the literature.

It is found that the optimal values of the FRP-to-BBR conversion factors derived from the AOD measurements are larger (by factors of about 2-3) and more uncertain than those derived from the CO measurements. This difference (which may be due to, e.g., underestimation of aerosol emission factors) is consistent with underestimation of aerosol emissions reported in the literature (Kaiser et al., 2012; Petrenko et al., 2012) but is found to be not statistically significant in this study. The larger uncertainty of the aerosol-derived FRP-to-BBR conversion factors is associated with much smaller contribution of the AOD measurements and simulations (compared to the contribution of the respective CO data) to the FRP-to-BBR conversion factor estimates derived from the combined optimization using both CO and AOD measurements. The possible underestimation of aerosol emission factors is reflected in the uncertainty range of our combined retrieval of the CO$_2$ emissions and is not likely to introduce a considerable positive bias in it. The ranges of uncertainty of the combined optimal estimates of the conversion factors (0.27 to 0.53 kg MJ^{-1} for forest fires and 0.26 to 0.74 kg MJ^{-1} for grass fires) are evaluated to be smaller compared to the uncertainties of the estimates based on one species alone and are found to include the independent estimates of the conversion factors (0.368 ± 0.015 kg MJ^{-1}) obtained by Wooster et al. (2005) in an analysis of experimental grass fires.

Special tests of our estimation procedure were conducted in order to examine the sensitivity of the estimates of the FRP-to-BBR conversion factors and CO$_2$ emissions to the assumed diurnal variations of FRP and to the parameterization of the maximum injection height. The results of these tests emphasized the importance of using the correct diurnal cycle of FRP for the estimation of the FRP-to-BBR conversion factors, but revealed almost no changes in the optimal estimates of the conversion factors obtained with a quite different parameterization of the maximum injection height. At the same time, the estimates of the total CO$_2$ emissions were found to be robust and rather insensitive to the examined changes in the estimation procedure.

The FRP-to-BBR conversion factors constrained by atmospheric measurements in 2012 were used to calculate the total CO$_2$ emissions from fires in the study region (50–76° N; 60–135° E) in the periods from 1 April to 30 September of several years (2007–2012). The estimates obtained were compared with the corresponding estimates provided by the GFASv1.0 and GFED3.1 biomass burning emission inventories. The pyrogenic CO$_2$ emissions in 2012 were estimated to be in the range from about 280 to 550 Tg C. This amount is eqivalent to about 60 to 110 % of the current estimates of the total fossil-fuel CO$_2$ emissions in Russia, indicating that open fires play a large role in the carbon balance of Eurasia. The obtained optimal estimate of the total CO$_2$ emissions in 2012 (392 Tg C) is about 73 % larger than the corresponding estimate provided by the GFASv1.0 emission data base (the GFED3.1 data for 2012 were not available). Considerable differences were also revealed between our estimates and the inventory data for other years (specifically, our indirect "top-down" estimates for the total biomass burning CO$_2$ emissions in the period from 2007 to 2011 in Siberia are by the factors of 1.8 and 2.5 larger than the corresponding alternative estimates), although all of the estimates demonstrate rather similar inter-annual variability.

Comparison of the spatial structures of the CO$_2$ emission estimates obtained in this study and provided by the GFASv1.0 and GFED3.1 emission inventories revealed that the correlation of our estimates with the results of both inventories is better than the correlation between the GFASv1.0 and GFED3.1 estimates. We consider this outcome as evidence that the overall uncertainties in our CO$_2$ emission estimates for Siberia do not exceed the uncertainties in the respective GFED3.1 and GFASv1.0 data.

We conclude that (1) the proposed general method for the estimation of CO$_2$ emissions from biomass burning allows getting reasonable and useful results by using available satellite measurements of CO and aerosol together with a chemistry-transport model; (2) the CO and aerosol emissions in Siberia are consistent with each other (taking into account their uncertainties) when assumed to be related through typical emission factors reported in the literature; and (3) the large discrepancies between the different estimates of CO$_2$ emissions indicate that the current knowledge of biomass burning processes and of associated perturbations in the carbon cycle in Siberia is very incomplete, and further dedicated studies are needed to identify the reasons for these discrepancies. We believe that a considerable reduction of uncertainties in the results of the method proposed here can be achieved by using satellite CO$_2$ measurements of major fire plumes to diagnose the ratios of emission of CO$_2$ and co-emitted species, as suggested by Silva et al. (2013) for the case of anthropogenic combustion emissions.

References

Akagi, S. K., Yokelson, R. J., Wiedinmyer, C., Alvarado, M. J., Reid, J. S., Karl, T., Crounse, J. D., and Wennberg, P. O.: Emission factors for open and domestic biomass burning for use in atmospheric models, Atmos. Chem. Phys., 11, 4039–4072, doi:10.5194/acp-11-4039-2011, 2011.

Andreae, M. O. and Merlet, P.: Emission of trace gases and aerosols from biomass burning, Global Biogeochem. Cy., 15, 955–966, doi:10.1029/2000GB001382, 2001.

Arellano Jr., A. F., Kasibhatla, P. S., Giglio, L., van der Werf, G. R., Randerson, J. T., and Collatz, G. J.: Time dependent inversion estimates of global biomass-burning CO emissions using Measurement of Pollution in the Troposphere (MOPITT) measurements, J. Geophys. Res., 111, D09303, doi:10.1029/2005JD006613, 2006.

Berezin, E. V., Konovalov, I. B., Ciais, P., Richter, A., Tao, S., Janssens-Maenhout, G., Beekmann, M., and Schulze, E.-D.: Multiannual changes of CO_2 emissions in China: indirect estimates derived from satellite measurements of tropospheric NO_2 columns, Atmos. Chem. Phys., 13, 9415–9438, doi:10.5194/acp-13-9415-2013, 2013.

Bessagnet, B., Hodzic, A., Vautard, R., Beekmann, M., Cheinet, S., Honoré, C., Liousse, C., and Rouil, L.: Aerosol modeling with CHIMERE – preliminary evaluation at the continental scale, Atmos. Environ., 38, 2803–2817, 2004.

Bessagnet, B., Menut, L., Curci, G., Hodzic, A., Guillaume, B., Liousse, C., Moukhtar, S., Pun, B., Seigneur, C., and Schulz, M.: Regional modeling of carbonaceous aerosols over Europe – focus on secondary organic aerosols, J. Atmos. Chem., 61, 175–202, 2009.

Bond, T. C., Doherty, S. J., Fahey, D. W., Forster, P. M., Berntsen, T., DeAngelo, B. J., Flanner, M. G., Ghan, S., Kärcher, B., Koch, D., Kinne, S., Kondo, Y., Quinn, P. K., Sarofim, M. C., Schultz, M. G., Schulz, M., Venkataraman, C., Zhang, H., Zhang, S., Bellouin, N., Guttikunda, S. K., Hopke, P. K., Jacobson, M. Z., Kaiser, J. W., Klimont, Z., Lohmann, U., Schwarz, J. P., Shindell, D., Storelvmo, T., Warren, S. G., and Zender, C. S.: Bounding the role of black carbon in the climate system: a scientific assessment, J. Geophys. Res.-Atmos., 118, 5380–5552, doi:10.1002/jgrd.50171, 2013.

Bond-Lamberty, B., Peckham, S. D., Ahl, D. E., and Gower, S. T.: Fire as the dominant driver of central Canadian boreal forest carbon balance, Nature, 450, 89–92, doi:10.1038/nature06272, 2007.

Brioude, J., Petron, G., Frost, G. J., Ahmadov, R., Angevine, W. M., Hsie, E.-Y., Kim, S.-W., Lee, S.-H., McKeen, S. A., Trainer, M., Fehsenfeld, F. C., Holloway, J. S., Peischl, J., Ryerson, T. B., and Gurney, K. R.: A new inversion method to calculate emission inventories without a prior at mesoscale: application to the anthropogenic CO_2 emission from Houston, Texas, J. Geophys. Res., 117, D05312, doi:10.1029/2011JD016918, 2012.

Chevallier, F., Engelen, R. J., Carouge, C., Conway, T. J., Peylin, P., Pickett-Heaps, C., Ramonet, M., Rayner, P. J., and Xueref-Remy, I.: AIRS-based versus flask-based estima-

tion of carbon surface fluxes, J. Geophys. Res., 114, D20303, doi:10.1029/2009JD012311, 2009.

Clerbaux, C., Boynard, A., Clarisse, L., George, M., Hadji-Lazaro, J., Herbin, H., Hurtmans, D., Pommier, M., Razavi, A., Turquety, S., Wespes, C., and Coheur, P.-F.: Monitoring of atmospheric composition using the thermal infrared IASI/MetOp sounder, Atmos. Chem. Phys., 9, 6041–6054, doi:10.5194/acp-9-6041-2009, 2009.

Dolman, A. J., Shvidenko, A., Schepaschenko, D., Ciais, P., Tchebakova, N., Chen, T., van der Molen, M. K., Belelli Marchesini, L., Maximov, T. C., Maksyutov, S., and Schulze, E.-D.: An estimate of the terrestrial carbon budget of Russia using inventory-based, eddy covariance and inversion methods, Biogeosciences, 9, 5323–5340, doi:10.5194/bg-9-5323-2012, 2012.

Dubovik, O., Lapyonok, T., Kaufman, Y. J., Chin, M., Ginoux, P., Kahn, R. A., and Sinyuk, A.: Retrieving global aerosol sources from satellites using inverse modeling, Atmos. Chem. Phys., 8, 209–250, doi:10.5194/acp-8-209-2008, 2008.

Chi, X., Winderlich, J., Mayer, J.-C., Panov, A. V., Heimann, M., Birmili, W., Heintzenberg, J., Cheng, Y., and Andreae, M. O.: Long-term measurements of aerosol and carbon monoxide at the ZOTTO tall tower to characterize polluted and pristine air in the Siberian taiga, Atmos. Chem. Phys., 13, 12271–12298, doi:10.5194/acp-13-12271-2013, 2013.

Ciais, P., Rayner, P., Chevallier, F., Bousquet, P., Logan, M., Peylin, P., and Ramonet, M.: Atmospheric inversions for estimating CO_2 fluxes: methods and perspectives, Climatic Change, 103, 69–92, 2010.

Conard, S., Sukhinin, A., Stocks, B., Cahoon, D., Davidenko, E., and Ivanova, G.: Determining effects of area burned and fire severity on carbon cycling and emissions in Siberia, Climatic Change, 55, 197–211, 2002.

EC-JRC/PBL (European Commission, Joint Research Centre/Netherlands Environmental Assessment Agency): Emission Database for Global Atmospheric Research (EDGAR), release version 4.2, available at: http://edgar.jrc.ec.europa.eu (last access: 3 January 2013), 2011.

Efron, B. and Tibshirani, R. J.: An Introduction to the Bootstrap, Chapman & Hall, London, Great Britain, 1993.

Enting, I. G.: Inverse Problems in Atmospheric Constituents Transport, Cambridge University Press, Cambridge, 2002.

Fokeeva, E. V., Safronov, A. N., Rakitin, V. S., Yurganov, L. N., Grechko, E. I., and Shumskii, R. A.: Investigation of the 2010 July–August fires impact on carbon monoxide atmospheric pollution in Moscow and its outskirts, estimating of emissions, Izv. Atmos. Ocean. Phy+., 47, 682–698, 2011.

Flemming, J., Peuch, V.-H., Engelen, R., and Kaiser, J. W.: A European global-to-regional air pollution forecasting system that combines modeling with satellite observations, EM Magazine, November 2013, 6–10, 2013.

Fortems-Cheiney, A., Chevallier, F., Pison, I., Bousquet, P., Carouge, C., Clerbaux, C., Coheur, P.-F., George, M., Hurtmans, D., and Szopa, S.: On the capability of IASI measurements to inform about CO surface emissions, Atmos. Chem. Phys., 9, 8735–8743, doi:10.5194/acp-9-8735-2009, 2009.

Giglio, L., Randerson, J. T., and van der Werf, G. R.: Analysis of daily, monthly, and annual burned area using the fourth-generation global fire emissions database (GFED4), J. Geophys. Res.-Biogeo., 118, 317–328, doi:10.1002/jgrg.20042, 2013.

Ginoux, P., Chin, M., Tegen, I., Prospero, J., Holben, B., Dubovik, O., and Lin, S.-J.: Sources and global distributions of dust aerosols simulated with the GOCART model, J. Geophys. Res., 106, 20255–20273, doi:10.1029/2000JD000053, 2001.

GLCF (The Global Land Cover Facility), Landsat GeoCover Degree Subset e010n000_LSATB_19900207, 1.0, University of Maryland Institute for Advanced Computer Studies, College Park, Maryland, 23 October 2001, 2005.

Guenther, A. B., Jiang, X., Heald, C. L., Sakulyanontvittaya, T., Duhl, T., Emmons, L. K., and Wang, X.: The Model of Emissions of Gases and Aerosols from Nature version 2.1 (MEGAN2.1): an extended and updated framework for modeling biogenic emissions, Geosci. Model Dev., 5, 1471–1492, doi:10.5194/gmd-5-1471-2012, 2012.

Gurney, K. R., Law, R. M., Denning, A. S., Rayner, P. J., Baker, D., Bousquet, Ph., Bruhwiler, L., Chen. Y.-H., Ciais, Ph., Fan, S., Fung, I. Y., Gloor, M., Heimann, M., Higuchi, K., John, J., Maki, T., Maksyutov, Sh., Masarie, K., Peylin, Ph., Prather, M., Pak, B. C., Randerson, J., Sarmiento, J., Taguchi, S., Takahashi, T., and Yuen, C.-W.: Towards robust regional estimates of CO$_2$ sources and sinks using atmospheric transport models, Nature, 415, 626–630, doi:10.1038/415626a, 2002.

Hansen, M. C. and Reed, B.: A comparison of the IGBP discover and University of Maryland 1 km global land cover products, Int. J. Remote Sens., 21, 1365–1373, 2000.

Hodnebrog, Ø., Solberg, S., Stordal, F., Svendby, T. M., Simpson, D., Gauss, M., Hilboll, A., Pfister, G. G., Turquety, S., Richter, A., Burrows, J. P., and Denier van der Gon, H. A. C.: Impact of forest fires, biogenic emissions and high temperatures on the elevated Eastern Mediterranean ozone levels during the hot summer of 2007, Atmos. Chem. Phys., 12, 8727–8750, doi:10.5194/acp-12-8727-2012, 2012.

Hodzic, A., Madronich, S., Bohn, B., Massie, S., Menut, L., and Wiedinmyer, C.: Wildfire particulate matter in Europe during summer 2003: meso-scale modeling of smoke emissions, transport and radiative effects, Atmos. Chem. Phys., 7, 4043–4064, doi:10.5194/acp-7-4043-2007, 2007.

Hooghiemstra, P. B., Krol, M. C., vanLeeuwen, T. T., van der Werf, G. R., Novelli, P. C., Deeter, M. N., Aben, I., and Röckmann, T.: Interannual variability of carbon monoxide emission estimates over South America from 2006 to 2010, J. Geophys. Res., 117, D15308, doi:10.1029/2012JD017758, 2012.

Horowitz, L. W., Walters, S., Mauzerall, D. L., Emmons, L. K., Rasch, P. J., Granier, C., Tie, X., Lamarque, J.-F., Schultz, M. G., Tyndall, G. S., Orlando, J. J., and Brasseur, G. P.: A global simulation of ozone and related tracers: description and evaluation of MOZART, version 2, J. Geophys. Res., 108, 4784, doi:10.1029/2002JD002853, 2003.

Houweling, S., Aben, I., Breon, F.-M., Chevallier, F., Deutscher, N., Engelen, R., Gerbig, C., Griffith, D., Hungershoefer, K., Macatangay, R., Marshall, J., Notholt, J., Peters, W., and Serrar, S.: The importance of transport model uncertainties for the estimation of CO$_2$ sources and sinks using satellite measurements, Atmos. Chem. Phys., 10, 9981–9992, doi:10.5194/acp-10-9981-2010, 2010.

Huijnen, V., Flemming, J., Kaiser, J. W., Inness, A., Leitão, J., Heil, A., Eskes, H. J., Schultz, M. G., Benedetti, A., Hadji-Lazaro, J., Dufour, G., and Eremenko, M.: Hindcast experiments of tropospheric composition during the summer 2010

fires over western Russia, Atmos. Chem. Phys., 12, 4341–4364, doi:10.5194/acp-12-4341-2012, 2012.

Huneeus, N., Chevallier, F., and Boucher, O.: Estimating aerosol emissions by assimilating observed aerosol optical depth in a global aerosol model, Atmos. Chem. Phys., 12, 4585-4606, doi:10.5194/acp-12-4585-2012, 2012.

Hungershoefer, K., Breon, F.-M., Peylin, P., Chevallier, F., Rayner, P., Klonecki, A., Houweling, S., and Marshall, J.: Evaluation of various observing systems for the global monitoring of CO$_2$ surface fluxes, Atmos. Chem. Phys., 10, 10503–10520, doi:10.5194/acp-10-10503-2010, 2010.

Hurtmans, D., Coheur, P.-F., Wespes, C., Clarisse, L., Scharf, O., Clerbaux, C., Hadji-Lazaro, J., George, M., and Turquety, S.: FORLI radiative transfer and retrieval code for IASI, J. Quant. Spectrosc. Ra., 113, 1391–1408, 2012.

IPCC: Climate change 2007: synthesis report, Contribution of Working Groups I, II and III to the Fourth Assessment Report of the Intergovernmental Panel on Climate Change, Core Writing Team, edited by: Pachauri, R. K. and Reisinger, A., IPPC, Geneva, Switzerland, 104 pp., 2007.

Ichoku, C. and Kaufman, J. Y: A method to derive smoke emission rates from MODIS fire radiative energy measurements, IEEE T. Geosci. Remote, 4311, 2636–2649, 2005.

Ichoku, C., Remer, L. A., and Eck, T. F.: Quantitative evaluation and intercomparison of morning and afternoon Moderate Resolution Imaging Spectroradiometer (MODIS) aerosol measurements from Terra and Aqua, J. Geophys. Res., 110, D10S03, doi:10.1029/2004JD004987, 2005.

Ichoku, C., Giglio, L., Wooster, M. J., and Remer, L. A.: Global characterization of biomass-burning patterns using satellite measurements of fire radiative energy, Remote Sens. Environ., 112, 2950–2962, doi:10.1016/j.rse.2008.02.009, 2008.

Ito, A.: Mega fire emissions in Siberia: potential supply of bioavailable iron from forests to the ocean, Biogeosciences, 8, 1679–1697, doi:10.5194/bg-8-1679-2011, 2011.

Jaffe, D. A. and Wigder, N. L.: Ozone production from wildfires: A critical review, Atmos. Environ., 51, 1–10, doi:10.1016/j.atmosenv.2011.11.063, 2012.

Jeong, J. I., Park, R. J., and Youn, D.: Effects of Siberian forest fires on air quality in East Asia during May 2003 and its climate implication, Atmos. Environ., 42, 8910–8922, doi:10.1016/j.atmosenv.2008.08.037, 2008.

Justice, C. O., Giglio, L., Korontzi, S., Owens, J., Morisette, J. T., Roy, D., Descloitres, J., Alleaume, S., Petitcolin, F., and Kaufman, Y.: The MODIS fire products, Remote Sens. Environ., 83, 244–262, 2002.

Kaiser, J. W., Flemming, J., Schultz, M. G., Suttie, M., and Wooster, M. J.: The MACC Global Fire Assimilation System: First Emission Products (GFASv0), Tech. Memo. 596, ECMWF, Reading, UK, 2009a.

Kaiser, J. W., Suttie, M., Flemming, J., Morcrette, J.-J., Boucher, O., and Schultz, M. G.: Global real-time fire emission estimates based on space-borne fire radiative power observations, AIP Conf. Proc., 1100, 645–648, 3–8 August 2008, Foz do Iguaçu (Brazil) 2009b.

Kaiser, J. W., Heil, A., Andreae, M. O., Benedetti, A., Chubarova, N., Jones, L., Morcrette, J.-J., Razinger, M., Schultz, M. G., Suttie, M., and van der Werf, G. R.: Biomass burning emissions estimated with a global fire assimilation sys-

tem based on observed fire radiative power, Biogeosciences, 9, 527–554, doi:10.5194/bg-9-527-2012, 2012.

Kaufman, Y. J., Tanre, D., Remer, L. A., Vermote, E. F., Chu, A., and Holben, B. N.: Operational remote sensing of tropospheric aerosol over land from EOS moderate resolution imaging spectroradiometer, J. Geophys. Res., 102, 17051–17067, 1997.

Kinne, S., Lohmann, U., Feichter, J., Schulz, M., Timmreck, C., Ghan, S., Easter, R., Chin, M., Ginoux, P., Takemura, T., Tegen, I., Koch, D., Herzog, M., Penner, J., Pitari11, G., Holben, B., Eck, T., Smirnov, A., Dubovik, O., Slutsker, I., Tanre, D., Torres, O., Mishchenko, M., Geogdzhayev, I., Chu, D. A., and Kaufman, Y.: Monthly averages of aerosol properties: a global comparison among models, satellite data, and AERONET ground data, J. Geophys. Res., 108, 4634, doi:10.1029/2001JD001253, 2003.

Konovalov, I. B., Beekmann, M., Kuznetsova, I. N., Yurova, A., and Zvyagintsev, A. M.: Atmospheric impacts of the 2010 Russian wildfires: integrating modelling and measurements of an extreme air pollution episode in the Moscow region, Atmos. Chem. Phys., 11, 10031–10056, doi:10.5194/acp-11-10031-2011, 2011.

Konovalov, I. B., Beekmann, M., D'Anna, B., and George, C.: Significant light induced ozone loss on biomass burning aerosol: evidence from chemistry-transport modeling based on new laboratory studies, Geophys. Res. Lett., 39, L17807, doi:10.1029/2012GL052432, 2012.

Krol, M., Peters, W., Hooghiemstra, P., George, M., Clerbaux, C., Hurtmans, D., McInerney, D., Sedano, F., Bergamaschi, P., El Hajj, M., Kaiser, J. W., Fisher, D., Yershov, V., and Muller, J.-P.: How much CO was emitted by the 2010 fires around Moscow?, Atmos. Chem. Phys., 13, 4737–4747, doi:10.5194/acp-13-4737-2013, 2013.

Kukavskaya, E. A., Soja, A. J., Petkov, A. P., Ponomarev, E. I., Ivanova, G. A., and Conard, S. G.: Fire emissions estimates in Siberia: evaluation of uncertainties in area burned, land cover, and fuel consumption, Can. J. Forest Res., 43, 493–506, doi:10.1139/cjfr-2012-0367, 2013.

Lamarque, J.-F., Bond, T. C., Eyring, V., Granier, C., Heil, A., Klimont, Z., Lee, D., Liousse, C., Mieville, A., Owen, B., Schultz, M. G., Shindell, D., Smith, S. J., Stehfest, E., Van Aardenne, J., Cooper, O. R., Kainuma, M., Mahowald, N., McConnell, J. R., Naik, V., Riahi, K., and van Vuuren, D. P.: Historical (1850–2000) gridded anthropogenic and biomass burning emissions of reactive gases and aerosols: methodology and application, Atmos. Chem. Phys., 10, 7017–7039, doi:10.5194/acp-10-7017-2010, 2010.

Langmann, B., Duncan, B., Textor, C., Trentmann, J., and van der Werf, G. R.: Vegetation fire emissions and their impact on air pollution and climate, Atmos. Environ., 43, 107–116, doi:10.1016/j.atmosenv.2008.09.047, 2009.

Larkin, N. K., O'Neill, S. M., Solomon, R., Raffuse, S., Strand, T., Sullivan, D. C., Krull, C., Rorig, M., Peterson, J. L., and Ferguson, S. A.: The BlueSky smoke modeling framework, Int. J. Wildland Fire, 18, 906–920, 2009.

Lloyd, J., Langenfelds, R. L., Francey, R. J., Gloor, M., Tchebakova, N. M., Zolotoukhine, D., Brand, W. A., Werner, R. A., Jordan, A., Allison, C. A., Zrazhewske, V., Shibistova, O., and Schulze, E.-D.: A trace-gas climatology above Zotino, central Siberia, Tellus B, 54, 749–767, 2002.

Lorenz, K. and Lal, R.: Carbon Sequestration in Forest Ecosystems, Springer, the Netherlands, 2010.

Menut, L., Bessagnet, B., Khvorostyanov, D., Beekmann, M., Blond, N., Colette, A., Coll, I., Curci, G., Foret, G., Hodzic, A., Mailler, S., Meleux, F., Monge, J.-L., Pison, I., Siour, G., Turquety, S., Valari, M., Vautard, R., and Vivanco, M. G.: CHIMERE 2013: a model for regional atmospheric composition modelling, Geosci. Model Dev., 6, 981–1028, doi:10.5194/gmd-6-981-2013, 2013.

Nassar, R., Jones, D. B. A., Kulawik, S. S., Worden, J. R., Bowman, K. W., Andres, R. J., Suntharalingam, P., Chen, J. M., Brenninkmeijer, C. A. M., Schuck, T. J., Conway, T. J., and Worthy, D. E.: Inverse modeling of CO$_2$ sources and sinks using satellite observations of CO$_2$ from TES and surface flask measurements, Atmos. Chem. Phys., 11, 6029–6047, doi:10.5194/acp-11-6029-2011, 2011.

Nenes, A., Pilinis, C., and Pandis, S.: ISORROPIA: a new thermodynamic model for inorganic multicomponent atmospheric aerosols, Aquat. Geochem., 4, 123–152, 1998.

Olivier, J. G. J., Berdowski, J. J. M., Peters, J. A. H. W., Bakker, J., Visschedijk, A. J. H., and en Bloos, J.-P. J.: Applications of EDGAR, Including a description of EDGAR 3.0: reference database with trend data for 1970–1995, RIVM report No 773301 001/NOP report No 410200 051, RIVM, Bilthoven, 142 pp., 2001.

Pak, B. C. and Prather, M. J.: CO$_2$ source inversion using satellite observations in the upper troposphere, Geophys. Res. Lett., 2824, 4571–4574, 2001.

Palmer, P. I., Suntharalingam, P., Jones, D. B. A., Jacob, D. J., Streets, D. G., Fu, Q. Y., Vay, S. A., and Sachse, G. W.: Using CO$_2$: CO correlations to improve inverse analyses of carbon fluxes, J. Geophys. Res., 111, D12318, doi:10.1029/2005JD006697, 2006.

Park, R. J., Jacob, D. J., Chin, M., and Martin, R. V.: Sources of carbonaceous aerosols over the United States and implications for natural visibility, J. Geophys. Res., 108, D4355, doi:10.1029/2002JD003190, 2003.

Pereira, G., Freitas, S. R., Moraes, E. C., Ferreira, N. J., Shimabukuro, Y. E., Rao, V. B., and Longo, K. M.: Estimating trace gas and aerosol emissions over South America: relationship between fire radiative energy released and aerosol optical depth observations, Atmos. Environ., 43, 6388–6397, 2009.

Petrenko, M., Kahn, R., Chin, M., Soja, A., Kucsera, T., and Harshvardhan: The use of satellite-measured aerosol optical depth to constrain biomass burning emissions source strength in the global model GOCART, J. Geophys. Res., 117, D18212, doi:10.1029/2012JD017870, 2012.

Pfister, G., Pétron, G., Emmons, L. K., Gille, J. C., Edwards, D. P., Lamarque, J.-F., Attie, J.-L., Granier, C., and Novelli, P. C.: Evaluation of CO simulations and the analysis of the CO budget for Europe, J. Geophys. Res., 109, D19304, doi:10.1029/2004JD004691, 2004.

Pfister, G., Hess, P. G., Emmons, L. K., Lamarque, J.-F., Wiedinmyer, C., Edwards, D. P., Pétron, G., Gille, J. C., and Sachse, G. W.: Quantifying CO emissions from the 2004 Alaskan wildfires using MOPITT CO data, Geophys. Res. Lett., 32, L11809, doi:10.1029/2005GL022995, 2005.

Pfister, G. G., Wiedinmyer, C., and Emmons, L. K.: Impacts of the fall 2007 California wildfires on surface ozone: integrating

local observations with global model simulations, Geophys. Res. Lett., 35, L19814, doi:10.1029/2008GL034747, 2008.

Press, W. H., Teukolsky, S. A., Vetterling, W. T., and Flannery, B. P.: Numerical Recipes, 2nd edn., Cambridge University Press, Cambridge, 1992.

Pun, B. K., Seigneur, C., and Lohman, K.: Modeling secondary organic aerosol formation via multiphase partitioning with molecular data, Environ. Sci. Technol., 40, 4722–4731, 2006.

Rayner, P. J., Law, R. M., Allison, C. E., Francey, R. J., Trudinger, C. M., and Pickett-Heaps, C.: Interannual variability of the global carbon cycle (1992–2005) inferred by inversion of atmospheric CO$_2$ and δ^{13}CO$_2$ measurements, Global Biogeochem. Cy., 22, GB3008, doi:10.1029/2007GB003068, 2008.

Reid, J. S., Eck, T. F., Christopher, S. A., Koppmann, R., Dubovik, O., Eleuterio, D. P., Holben, B. N., Reid, E. A., and Zhang, J.: A review of biomass burning emissions part III: intensive optical properties of biomass burning particles, Atmos. Chem. Phys., 5, 827–849, doi:10.5194/acp-5-827-2005, 2005.

Remer, L. A., Kaufman, Y. J., Tanre, D., Mattoo, S., Chu, D. A., Martins, J. V., Li, R.-R., Ichoku, C., Levy, R. C., Kleidman, R. G., Eck, T. F., Vermote, E., and Holben, B. N.: The MODIS aerosol algorithm, products, and validation, J. Atmos. Sci., 62, 947–973, 2005.

R'Honi, Y., Clarisse, L., Clerbaux, C., Hurtmans, D., Duflot, V., Turquety, S., Ngadi, Y., and Coheur, P.-F.: Exceptional emissions of NH$_3$ and HCOOH in the 2010 Russian wildfires, Atmos. Chem. Phys., 13, 4171–4181, doi:10.5194/acp-13-4171-2013, 2013.

Rivier, L., Ciais, P., Hauglustaine, D. A., Bakwin, P., Bousquet, P., Peylin, P., and Klonecki, A.: Evaluation of SF$_6$, C$_2$Cl$_4$, and CO to approximate fossil fuel CO$_2$ in the Northern Hemisphere using a chemistry transport model, J. Geophys. Res., 111, D16311, doi:10.1029/2005JD006725, 2006.

Robinson, A. L., Donahue, N. M., Shrivastava, M. K., Weitkamp, E. A., Sage, A. M., Grieshop, A. P., Lane, T. E., Pierce, J. R., and Pandis, S. N.: Rethinking organic aerosols: Semivolatile emissions and photochemical aging, Science, 315(5816), 1259-1262, doi:10.1126/science.1133061, 2007.

Saeki, T., Maksyutov, S., Saito, M., Valsala, V., Oda, T., Andres, R. J., Belikov, D., Tans, P., Dlugokencky, E., Yoshida, Y., Morino, I., Uchino, O., and Yokota, T.: Inverse modeling of CO$_2$ fluxes using GOSAT data and multi-year ground-based observations, SOLA, 9, 45–50, 2013.

Schmidt, H., Derognat, C., Vautard, R., and Beekmann, M.: A comparison of simulated and observed ozone mixing ratios for the summer of 1998 in Western Europe, Atmos. Environ., 36, 6277–6297, 2001.

Schutgens, N., Nakata, M., and Nakajima, T.: Estimating aerosol emissions by assimilating remote sensing observations into a global transport model, Remote Sens., 4, 3528–3543, doi:10.3390/rs4113528, 2012.

Schulze, E.-D., Vygodskaya, N. N., Tchebakova, N. M., Czimczik, C. I., Kozlov, D. N., Lloyd, J., Mollicone, D., Parfenova, E., Sidorov, K. N., Varlagin, A. V., and Wirth, C.: The Eurosiberian Transect: an introduction to the experimental region, Tellus B, 54, 5, 421–428, 2002.

Schulze, E.-D., Wirth, C., Mollicone, D., von Lüpke, N., Ziegler, W., Achard, F., Mund, M., Prokushkin, A., and Scherbina, S.: Factors promoting larch dominance in central Siberia: fire versus growth performance and implications for carbon dynamics at the boundary of evergreen and deciduous conifers, Biogeosciences, 9, 1405–1421, doi:10.5194/bg-9-1405-2012, 2012.

Shvidenko, A. Z., Shchepashchenko, D. G., Vaganov, E. A., Sukhinin, A. I., Maksyutov, Sh. Sh., McCallum, I., and Lakyda, I. P.: Impact of wildfire in Russia between 1998–2010 on ecosystems and the global carbon budget, Dokl. Earth Sci., 441, 2, 1678–1682, 2011.

Silva, S. J., Arellano, A. F., and Worden H.: Toward anthropogenic combustion emission constraints from space-based analysis of urban CO2/CO sensitivity, Geophys. Res. Lett., 40, 4971–4976, doi:10.1002/grl.50954, 2013.

Singh, H. B., Cai, C., Kaduwela, A., Weinheimer, A. J., and Wisthaler, A.: Interactions of fire emissions and urban pollution over California: ozone formation and air quality simulations, Atmos. Environ., 56, 45–51, 2012.

Skamarock, W. C., Klemp, J. B., Dudhia, J., Gill, D. O., Barker, D. M., Wang, W., and Powers, J. G.: A description of the Advanced Research WRF Version 2, NCAR Tech Notes-468+STR, 2005.

Soja, A. J., Cofer, W. R., Shugart, H. H., Sukhinin, A. I., Stackhouse Jr., P. W., McRae, D. J., and Conard, S. G.: Estimating fire emissions and disparities in boreal Siberia (1998–2002), J. Geophys. Res., 109, D14S06, doi:10.1029/2004JD004570, 2004.

Sofiev, M., Vankevich, R., Lotjonen, M., Prank, M., Petukhov, V., Ermakova, T., Koskinen, J., and Kukkonen, J.: An operational system for the assimilation of the satellite information on wildland fires for the needs of air quality modelling and forecasting, Atmos. Chem. Phys., 9, 6833–6847, doi:10.5194/acp-9-6833-2009, 2009.

Sofiev, M., Ermakova, T., and Vankevich, R.: Evaluation of the smoke-injection height from wild-land fires using remote-sensing data, Atmos. Chem. Phys., 12, 1995–2006, doi:10.5194/acp-12-1995-2012, 2012.

Sofiev, M., Vankevich, R., Ermakova, T., and Hakkarainen, J.: Global mapping of maximum emission heights and resulting vertical profiles of wildfire emissions, Atmos. Chem. Phys., 13, 7039–7052, doi:10.5194/acp-13-7039-2013, 2013.

Suntharalingam, P., Jacob, D. J., Palmer, P. I., Logan, J. A., Yantosca, R. M., Xiao, Y., Evans, M. J., Streets, D. G., Vay, S. L., and Sachse, G. W.: Improved quantification of Chinese carbon fluxes using CO$_2$/CO correlations in Asian outflow, J. Geophys. Res., 109, D18S18, doi:10.1029/2003JD004362, 2004.

Tarantola, A.: Inverse Problem Theory: Methods for Data Fitting and Model Parameter Estimation, Elsevier, Amsterdam, 1987.

Turquety, S., Logan, J. A., Jacob, D. J., Hudman, R. C., Leung, F. Y., Heald, C. L., Yantosca, R. M., Wu, S., Emmons, L. K., Edwards, D. P., and Sachse, G. W.: Inventory of boreal fire emissions for North America in 2004: the importance of peat burning and pyro-convective injection, J. Geophys. Res., 112, D12S03, doi:10.1029/2006JD007281, 2007.

Turquety, S., Hurtmans, D., Hadji-Lazaro, J., Coheur, P.-F., Clerbaux, C., Josset, D., and Tsamalis, C.: Tracking the emission and transport of pollution from wildfires using the IASI CO retrievals: analysis of the summer 2007 Greek fires, Atmos. Chem. Phys., 9, 4897–4913, doi:10.5194/acp-9-4897-2009, 2009.

van der Werf, G. R., Randerson, J. T., Giglio, L., Collatz, G. J., Mu, M., Kasibhatla, P. S., Morton, D. C., DeFries, R. S.,

Jin, Y., and van Leeuwen, T. T.: Global fire emissions and the contribution of deforestation, savanna, forest, agricultural, and peat fires (1997–2009), Atmos. Chem. Phys., 10, 11707–11735, doi:10.5194/acp-10-11707-2010, 2010.

Vautard, R., Bessagnet, B., Chin, M., and Menut, L.: On the contribution of natural Aeolian sources to particulate matter concentrations in Europe: testing hypotheses with a modelling approach, Atmos. Environ., 39, 3291–3303, 2005.

Vermote, E., Ellicott, E., Dubovik, O., Lapyonok, T., Chin, M., Giglio, L., and Roberts, G. J.: An approach to estimate global biomass burning emissions of organic and black carbon from MODIS fire radiative power, J. Geophys. Res., 114, D18205, doi:10.1029/2008JD011188, 2009.

Wang, J., Christopher, S. A., Nair, U. S., Reid, J. S., Prins, E. M., Szykman, J., and Hand, J. L.: Mesoscale modeling of Central American smoke transport to the United States: 1. "Top-down" assessment of emission strength and diurnal variation impacts, J. Geophys. Res., 111, D05S17, doi:10.1029/2005JD006416, 2006.

Wiedinmyer, C., Quayle, B., Geron, C., Belote, A., McKenzie, D., Zhang, X., O'Neill, S., and Wynne, K. K.: Estimating emissions from fires in North America for air quality modeling, Atmos. Environ., 40, 3419–3432, doi:10.1016/j.atmosenv.2006.02.010, 2006.

Wiedinmyer, C., Akagi, S. K., Yokelson, R. J., Emmons, L. K., Al-Saadi, J. A., Orlando, J. J., and Soja, A. J.: The Fire INventory from NCAR (FINN): a high resolution global model to estimate the emissions from open burning, Geosci. Model Dev., 4, 625–641, doi:10.5194/gmd-4-625-2011, 2011.

Wooster, M. J., Roberts, G., Perry, G. L. W., and Kaufman, Y. J.: Retrieval of biomass combustion rates and totals from fire radiative power observations: FRP derivation and calibration relationships between biomass consumption and fire radiative energy release, J. Geophys. Res., 110, D24311, doi:10.1029/2005JD006318, 2005.

Xu, X., Wang, J., Henze, D. K., Qu, W., and Kopacz, M.: Constraints on aerosol sources using GEOSChem adjoint and MODIS radiances, and evaluation with multisensor (OMI, MISR) data, J. Geophys. Res.-Atmos., 118, 6396–6413, doi:10.1002/jgrd.50515, 2013.

Zhang, S., Penner, J. E., and Torres, O.: Inverse modeling of biomass burning emissions using Total Ozone Mapping Spectrometer aerosol index for 1997, J. Geophys. Res., 110, D21306, doi:10.1029/2004JD005738, 2005.

Table 1. Biomass burning emission factors (β, $\mathrm{g\,kg^{-1}}$) used in Eq. (1), their geometric standard deviation (σ_g, given in the round brackets), and the respective uncertainty range (given in the square brackets in terms of 1-σ_g interval) for different types of vegetative land cover. The data are based on Andreae and Merlet (2001) and subsequent updates.

	agricultural burning	grassland	extratropical forest
CO_2	1473 (1.21) [1217;1782]	1653 (1.05) [1574;1736]	1559 (1.08) [1444;1684]
CO	95 (1.90) [50;181]	64 (1.35) [47;86]	115 (1.43) [80;164]
OC	4.2 (2.00) [2.1;8.4]	3.2 (1.47) [2.2;4.7]	9.6 (1.60) [6.0;15.4]
BC	0.42 (1.90) [0.22;0.79]	0.47 (1.42) [0.33;0.66]	0.50 (1.46) [0.34;0.73]

Table 2. Estimates of the FRP-to-BBR conversion factors $(\mathrm{kg\,MJ^{-1}})$ for forest and grass (including agricultural) fires. The estimates derived independently from CO and AOD measurements by using the different model run settings are shown along with the combined optimal estimates. The geometric standard deviations characterizing uncertainties and the corresponding uncertainty ranges are given in round and square brackets, respectively.

Model run settings	CO		AOD		Combined	
	forest	grass	forest	grass	forest	grass
Fires_base	0.30 (1.49) [0.20;0.45]	0.30 (1.86) [0.17;0.60]	0.66 (1.86) [0.37;1.25]	0.86 (2.30) [0.34; 2.14]	0.38 (1.40) [0.27;0.53]	0.44 (1.69) [0.26;0.74]
Fires_test1	0.31 (1.48) [0.21;0.45]	0.31 (1.91) [0.16;0.59]	0.67 (1.91) [0.35;1.28]	0.83 (2.24) [0.37;1.87]	0.40 (1.42) [0.27;0.53]	0.45 (1.69) [0.27;0.76]
Fires_test2	0.52 (1.52) [0.34;0.79]	0.30 (2.06) [0.15;0.61]	0.85 (1.92) [0.44;1.66]	0.69 (2.94) [0.23;2.03]	0.60 (1.42) [0.42;0.85]	0.38 (1.86) [0.21;0.71]

Table 3. Optimal estimates of the CO$_2$ emissions (Tg C) from forest and grass (including agricultural) fires in Siberia in 2012. Different estimates are obtained from outputs of model runs and inversions with different settings. The geometric standard deviations characterizing uncertainties and the corresponding uncertainty ranges are given in round and square brackets, respectively.

| Model run settings/ inversion settings		forest	grass	total
Fires_base	CO- and AOD-based	257 (1.43) [180;366]	136 (1.71) [79;232]	392 (1.40) [280;550]
	CO-based	203 (1.52) [133;309]	93 (1.93) [48;179]	295 (1.50) [196;444]
	AOD-based	447 (1.88) [237;842]	264 (2.34) [113;617]	711 (1.80) [395;1280]
Fires_test1	CO- and AOD-based	255 (1.42) [179;362]	138 (1.70) [81;236]	393 (1.40) [281;551]
	CO-based	205 (1.51) [137;310]	94 (1.94) [48;183]	300 (1.50) [200;450]
	AOD-based	451 (1.94) [233;874]	256 (2.28) [112;583]	707 (1.81) [390;1281]
Fires_test2	CO- and AOD-based	261 (1.45) [181;378]	95 (1.88) [50;178]	356 (1.44) [248;512]
	CO-based	225 (1.55) [145;349]	74 (2.09) [35;155]	299 (1.54) [195;460]
	AOD-based	371 (1.95) [191;720]	170 (3.00) [57;512]	542 (1.98) [276;1063]
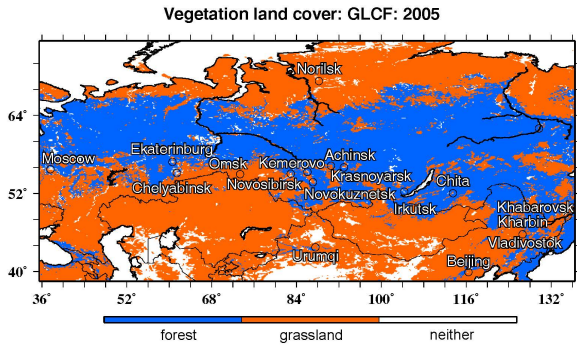
Fig. 1. Spatial distributions of the two vegetation land-cover aggregated categories considered in this study: forest (blue), and grassland including agricultural land (red). The pixels where a dominant category is neither forest nor grassland are left blank. The plots are based on GLCF (2005) data re-gridded with a resolution of $0.2° \times 0.1°$.

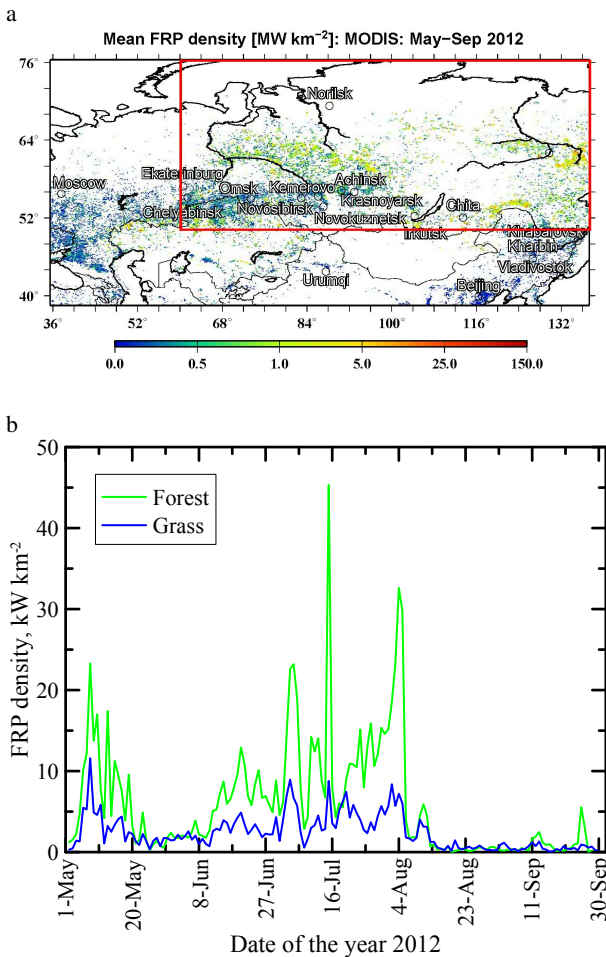**Fig. 2.** Average values of the daily maxima of the FRP density derived from the MODIS measurements: **(a)** spatial structure over the period chosen for data assimilation (from May to September 2012), **(b)** daily variations averaged over the region considered in this study (indicated by a red rectangle in **a**).
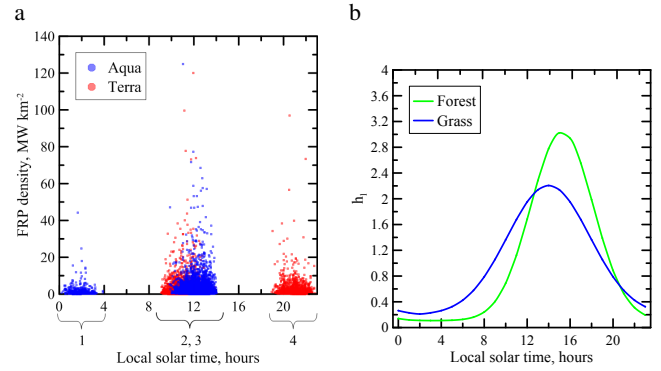
Fig. 3. (a) Daily maximum FRP densities derived from the MODIS measurements on board the AQUA and TERRA satellites over the study region (see red rectangle in Fig. 2a) as a function of the local solar time in May–September 2012; each point represents one selected measurement in a grid cell of $0.2° \times 0.1°$. Note that due to variable observation conditions and a low temporal resolution of the MODIS measurements, the daily maximum of FRP from a given fire is not necessarily always detected at the time of day when the actual FRP is largest. **(b)** Estimated regional average diurnal variations of FRP.
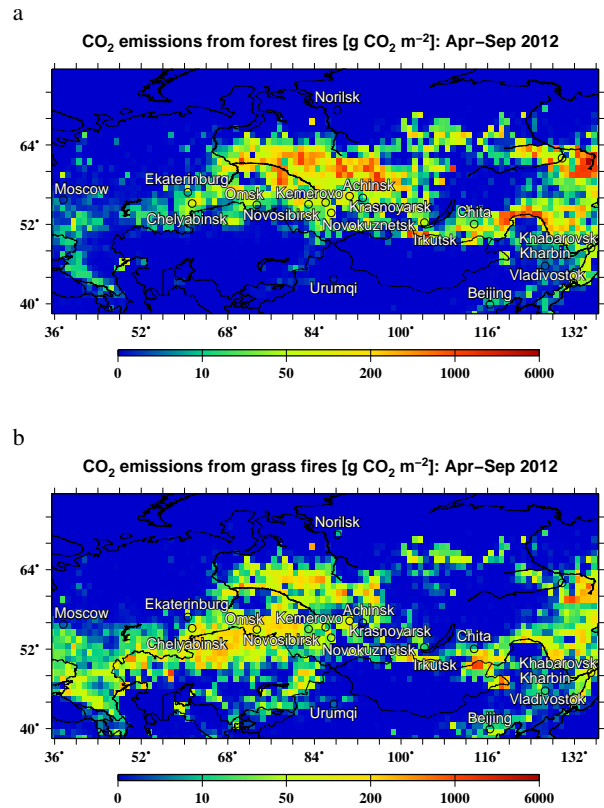

Fig. 4. CO$_2$ biomass burning emissions $(\mathrm{g\,CO_2\,m^{-2}})$ from **(a)** forests and **(b)** from other types of vegetative land cover (mainly grasslands): mean values estimated in this study for the period from April to September 2012.
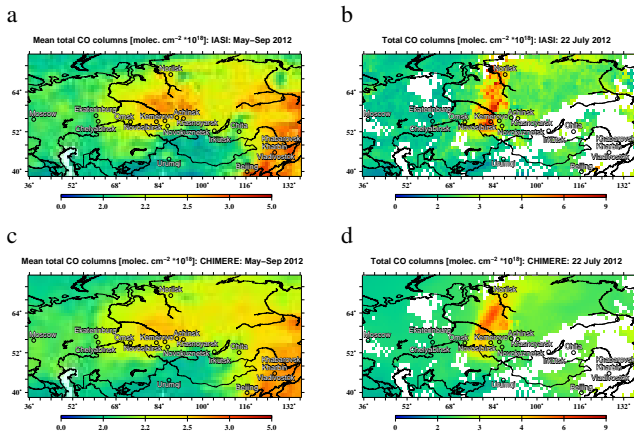
Fig. 5. Spatial distributions of the total CO columns according to **(a, b)** IASI measurements and **(c, d)** simulations after removing the bias not associated with fire emissions: **(a, c)** mean values over the modelled period (May–September 2012), **(b, d)** daily values for a selected day (22 July 2012). The measurements and simulations shown were withheld from the emission estimation procedure (see Sect. 4 for details).
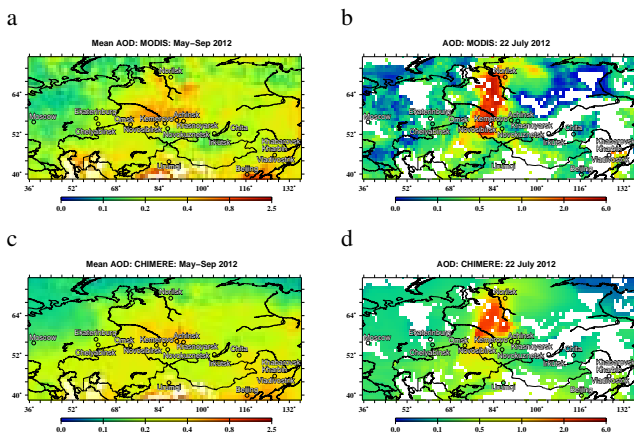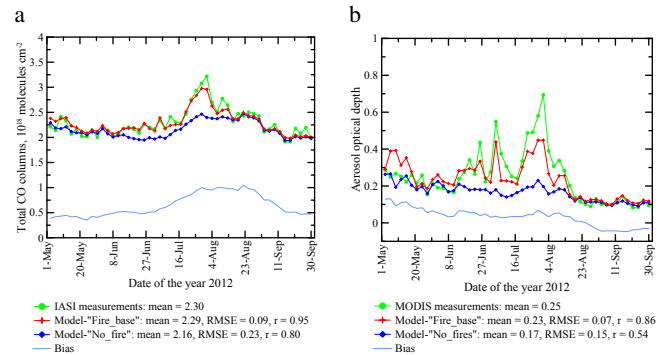

Fig. 7. Time series of **(a)** daily total CO columns and **(b)** AOD simulated by CHIMERE with ("Fires_base") and without ("No_fires") fire emissions in comparison to the data from the corresponding IASI and MODIS measurements. The measurements and simulations for the days shown were withheld from the emission estimation procedure. The simulations are presented after debiasing. Note that the indicated bias represents the values of Δ (see Sect. 2.3) taken with the opposite sign. All values are the averages over the Siberian study region.

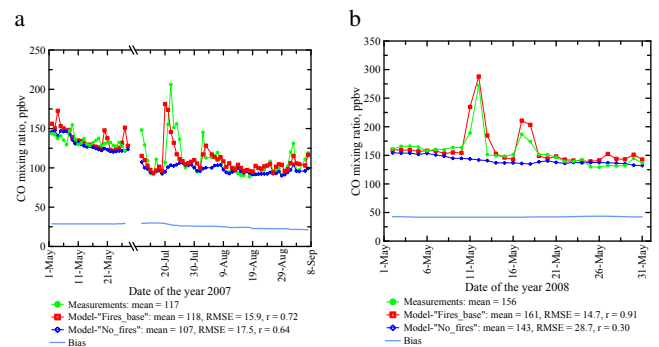**Fig. 6.** Same as in Fig. 5 but for AOD values.

Fig. 8. Comparison of the daily mean CO concentrations measured at the ZOTTO monitoring site with corresponding simulations (after debiasing) performed by CHIMERE without ("No_fires") and with ("Fires_base") fire emissions: the data are for the years **(a)** 2007 and **(b)** 2008. The "bias" shown by the solid blue line was estimated as the running average (over 30 days) of the difference between the measurements and simulations in the "No_fires" case for the days when the impact of fires was negligible (when the difference between the simulated concentrations in the "Fires_base" and "No_fires" did not exceed 10 %); all other days (with noticeable contribution of fires) were used for evaluation of the statistics reported below the figures.
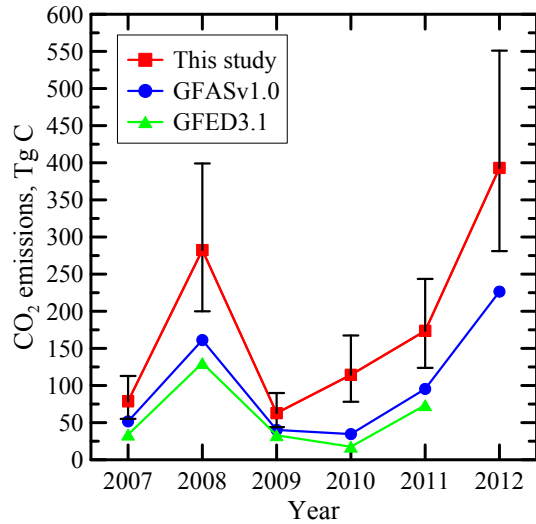
Fig. 9. Annual biomass burning CO_2 emissions (Tg C) in Siberia according to this study, GFASv1.0, and GFED3.1.

Fig. 10. Spatial distribution of the total CO_2 emissions $(g\,CO_2\,m^{-2})$ over the period April–September 2008: **(a)** this study, **(b)** GFASv1.0, **(c)** GFED3.1.
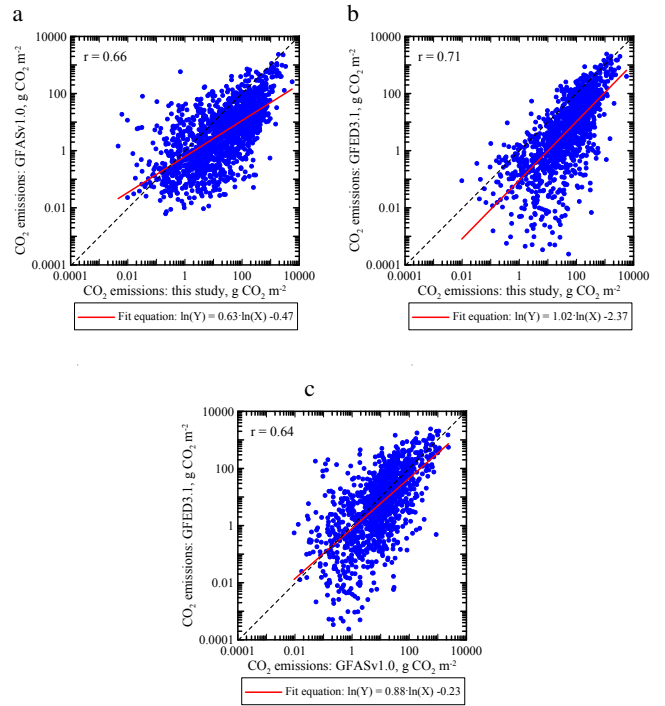

Fig. 11. Scatter plots of the gridded CO_2 emissions (see Fig. 10) estimated in this study and obtained from the GFASv1.0 and GFED3.1 inventories for the year 2008. The correlation coefficients (shown on the plots) are calc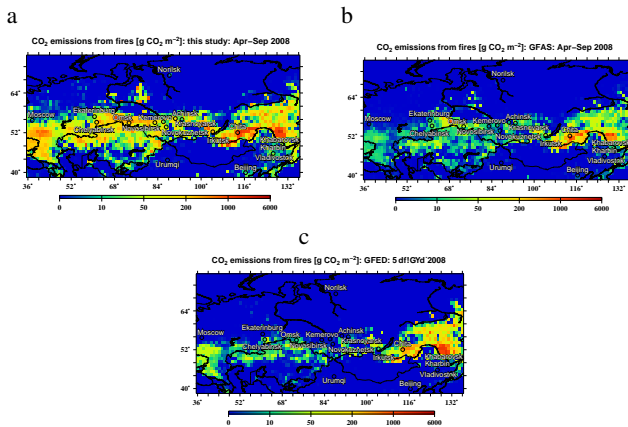ulated for the logarithms of the emission values.